2009-01-01

Additive Layer Manufacturing Of TI-6AL-4V By Electron Beam Melting From Powder Particles: Solid, Mesh And Foam Components Study

Sara M. Gaytan
University of Texas at El Paso, smgaytan@miners.utep.edu

ADDITIVE LAYER MANUFACTURING OF TI-6AL-4V BY ELECTRON BEAM MELTING FROM POWDER PARTICLES: SOLID, MESH AND FOAM COMPONENTS STUDY

SARA MARISELA GAYTAN GUILLEN

Department of Metallurgical and Materials Engineering

APPROVED:

Lawrence E. Murr, Ph.D., Chair

Stephen W. Stafford, Ph.D.

Ryan B. Wicker, Ph.D.

Patricia D. Witherspoon, Ph.D.
Dean of the Graduate School

Dedicated to my family

ADDITIVE LAYER MANUFACTURING OF TI-6AL-4V BY ELECTRON BEAM MELTING FROM POWDER PARTICLES: SOLID, MESH AND FOAM COMPONENTS STUDY

by

SARA MARISELA GAYTAN GUILLEN, BS

THESIS

Presented to the Faculty of the Graduate School of

The University of Texas at El Paso

in Partial Fulfillment

of the Requirements

for the Degree of

MASTER OF SCIENCE

Department of Metallurgical and Materials Engineering

THE UNIVERSITY OF TEXAS AT EL PASO

December 2009

ACKNOWLEDGEMENTS

I would like to thank my advisor Dr. Murr who has given me the opportunity to learn from his expertise. It is a pleasure and a privilege to be guided by such a recognized person. It has been an honor to be trained under his knowledge. I also want to thank all the faculty department of Metallugical and Materials Engineering, every professor I have had class with has left a valuable mark in my development as student. And special thanks to Mr. David Brown; it is fair to say that without him most of the project could not have been completed. I gratefully state the support given by the W. M. Keck Center for 3D Innovation at UTEP for providing the samples for the project.

I want to state the gratitude to my colleagues, coworkers and beloved friends Maribel Lopez, Brenda Machado, Diana Ramirez, Edwin Martinez, Louie Martinez, Daniel Hernandez, and Frank Medina, without them the project would not have been as fun and easy-going as it has been. And finally, I want to thank my entire family and Mr. Alejandro Valdez for all the love, support and patience provided every day of this journey.

Thank you!!

ABSTRACT

Additive Manufacturing by Electron Beam Melting Rapid Manufacturing is a technology that consists of the fabrication of a CAD design by melting powder particles in a layer by layer fashion. In this study, Ti-6Al-4V has been utilized to fabricate solid, mesh and foam components by EBM technologies. Powder analysis of Ti-6Al-4V was performed to obtain a better understanding of the porosity obtained by the system. After proper optimization of the machine, and porosity control, microstructural analysis was performed to the components already mentioned and correlated by transmission electron microscopy. Besides the microstructural analysis, tensile and hardness testing was performed to the components. Variations in density, and/or wall thickness of the components result in a variance in cooling rates that provide differences in microstructure and hardness discussed in this thesis. As a result, and mainly due to the astonishing properties obtained by these components a wide variety of fields can be benefited from these technologies.

TABLE OF CONTENTS

LIST OF TABLES

LIST OF FIGURES

CHAPTER 1

INTRODUCTION

The focus of this thesis was to analyze the characteristics of components fabricated by rapid prototyping through electron beam melting, more specifically the ARCAM A2 EBM system, from a metallurgical aspect. It is implied that specimens (designed and built by Francisco Medina, M. S., at the W. M. Keck Center for 3D Innovation at UTEP) coming out of this amazing machine have gone through Light Optical Metallography (LOM), and analyzed by scanning and transmission electron microscopy (SEM and TEM) as well as hardness and tensile testing. It is valid to say that the spectacular aspect of this technology remains in the fact that it is computer driven. This means that, for this research program, anything that can be created in a computer aided design (CAD) program can be built in a layer by layer fashion out of Ti-6Al-4V or other metal powder as long as the design does not exceed the minimum resolution of the system, which is roughly 0.1 millimeters in the z-direction and 0.5 millimeters in the x and y directions.

An analysis of the specimens at different parameters of the system, such as beam current, focus, scan rate, and scan sequencing, was the beginning of the project. Besides analyzing the samples at different parameters, it is important to mention that Ti-6Al-4V powder at different stages of the process was also chemically analyzed to obtain a further understanding of the alloy behavior. Once the optimal fabrication parameters were achieved, different sets of components were fabricated for analysis purposes.

Besides analyzing solid specimens, it is important to mention that, different densities were achieved for components created of the same size. The creation of designs that allow the manufacture of foam-like or cellular mesh specimens was possible with the aid of the software packages such as Netfabb Studio Professional 4.1 and Build Assembler 3.0. Mesh components built out of single unit geometries in a repeated fashion also created different types of specimens analyzed in this project. Several of these components had exactly the same dimensions but different densities. It is fair to say that this titanium alloy's foam or mesh components have a high potential application as a consequence of their light weight and exceptional, isotropic mechanical properties and corrosion resistance.

Being that Ti-6Al-4V is an alloy that is usually used for bone implant as well as aerospace applications, it is important to mention that this technology could widely be used to benefit them, and possibly other areas, to create components specific to the customer. However, there are few if any standards or certifications for electron beam melting (EBM) manufacturing or product development, unlike the conventional manufacturing processes from commercial material such as cast, wrought, or forged.

Another important aspect analyzed for this project is the analysis of quality control strategies and or/material certification. When manufacturing high precision, multiaxis, biomedical and aeronautical/aerospace components it is usually done from CNC machining from wrought forgings or cast ingots which meet established specifications. At the time of the creation of these components, an 85% of waste which is not necessary recycled is created [1,2]. Moreover, traditional machining often adds a significant cost since complex structures must be fabricated separately and then joined, especially enclosed or embedded

features. In addition, light weighting can be achieved by metal foam technologies which are difficult or impossible to integrate with monolithic, fully dense, functional products [3].

The fabrication of complex shapes and custom designed components from commercially available, atomized powders can be fabricated by various forms of additive layered manufacturing (ALM) recently developed [4,5,6]. Computer controlled or CAD is the building drive of these rapid prototyping or direct digital manufacturing technologies, which fabricate components by melting the powder layers using laser or electron beams.

This thesis explains applied research involving the manufacture of Ti-6Al-4V components by EBM and the concern of optimizing ALM-EBM building parameters as well as the analysis by optical and electron microscopy of metallography and build defects as well as the residual microstructures associated with measured mechanical behavior. In addition, powder and build chemistry have been analyzed for recycling purposes. Finally, a preliminary quality control characterization as a precursor to product certification and standards development for solid, mesh and integrated solid/mesh builds has been conducted.

CHAPTER 2

BACKGROUND

2.1 Titanium

Titanium is one of the metals more abundant in the earth's crust, following aluminum, iron and magnesium. Due to its porous and sponge-like appearance, it is usually called "sponge". This metal goes through four major steps to become this finished product form from ore. These four steps consist in the reduction of titanium ore to this porous form named "sponge", the melting of this "sponge" to form an ingot, then the conversion of these ingots into general mill products and finally the fabrication of finished shapes from the mill products. Titanium is obtained by the production of titanium tetrachloride ($TiCl_4$) and its reduction to titanium by either one of two different processes: Kroll process, which consists in the interaction with magnesium, or the Hunter process, which refers to the interaction with sodium [7]. The main cost for titanium processing is the use of $TiCl_4$, having 52% in a relative proportion of the cost. $TiCl_4$ is used in both the distillation and reduction processes to purify and produce metallic titanium. [8].

It is of great interest to know that titanium, especially in alloys, can be used in many applications due to the astonishing properties provided by the same. Because the properties of titanium are easily influenced by alloying elements and impurities, it is possible for this element to serve a wide range of applications with a minimum number of grades or alloys. As an example, Table 1.1 shows the tensile properties of an annealed titanium sheet as influenced by oxygen and iron impurity contents just to show the

importance of the alloying and impurity elements [7]. An interesting fact about titanium is that, although it can cause allergies or toxic response in one out of ten people it is widely used in several brands of candy as titanium dioxide: as an example is the coating of M&M's and Skittles as well as several toothpaste brands [9].

Table 2.11. Percent impurity content and the tensile properties obtained [7]

	Max. impurity content, %		Minimum tensile strength		Minimum yield strength at 0.2% offset	
Material	**Oxygen**	**Iron**	**Mpa**	**ksi**	**Mpa**	**ksi**
Ti-6Al-4V	0.2	0.3	925	134	870	126
Ti-6Al-4V ELI	0.13	0.25	900	130	830	120

2.2 Some Ti-6Al-4V Applications

Biomedical, automotive, sports and appearance related areas are some of the applications for titanium. Nevertheless, our interest is specifically in a special alloy: Ti-6Al-4V. This alloy provides a high fatigue strength as well as tolerable temperature capability, and therefore it could be used as connecting rods in the automotive field. A simple example in the sports field is how golf club heads of Ti-6Al-4V are obtained by investment casting. Another use given to titanium can be focused in jewelry and decorative arts as well applications where its natural gray-like appearance is desired, such as in roofs and domes. Finally, the most relevant application for this study is the use of Ti-6Al-4V in the biomedical field. This alloy is specially used for applications requiring high fatigue strength, such as the stem of a hip joint implant, as well as in the metal backed shell and the screws. [8].

Titanium and its alloys can be the best selection as for biomaterials for orthopedic and dental implants since they have excellent mechanical properties, like fatigue resistance, high resistance to generalized and localized corrosion, biocompatibility such as good compatibility with human tissue [10,11].

Ti-6Al-4V is an alloy typically utilized as an orthopedic implant. It has been studied and results have shown that the alloy is tolerated by blood, indicating that this alloy, besides being suitable for orthopedics, can also be used in the cardiovascular field. After reviewing clinical, radiologic and laboratory records it was found that titanium does not have a harmful effect on local tissue surrounding the titanium implants. On the other hand, the downside of this alloy is the aluminum release being involved in neurological and metabolic-bone disease [9].

2.3 Aluminum and Vanadium

Ti-6Al-4V is composed of grains of two phases: known as alpha (α) and beta (β), which are hexagonal closed packed (HCP) and body centered cubic (BCC) crystal structures, respectively. Ti-6Al-4V at room temperature consists in the HCP crystal structure and when heated above the phase transformation temperature of 883°C it transforms to BCC structure [12,13]. Now, going a little bit deeper into the literature regarding Ti-6Al-4V, it is known that aluminum is a strong α stabilizer which means that as you increase the aluminum content the α/β transformation temperature will increase. One reason why aluminum is used is due to the fact that it also has a large solubility in α as well as in β phase, therefore providing a density reduction of the alloy [7]. While aluminum is

an α stabilizer, vanadium is a β isomorphous stabilizer that will decrease the α/β transition temperature in pure titanium, being completely miscible in the β phase [7,8]. Furthermore, Ti-6Al-4V is an α/β alloy with up to 15 vol% β phase in equilibrium at 800°C, providing a balance of strength, ductility, fatigue and fracture properties, this alloy can be used at a maximum temperature of about 300°C. In addition, the Ti-6Al-4V ELI (extra low interstitial) provides good damage tolerance properties as well as high fracture toughness [8].

2.4 Manufacturing

Conventional manufacturing goes from different types of casting, forging, extrusion, machining, and Vacuum Arc Remelting (VAR) among others, being the last one a process usually utilized for titanium alloys since it prevents reactions with the melting crucible [14]. Many finishing methods can be used to produce a final product, specially for implants, such as finish machining, finish grinding, wire or sink EDM (electrical discharge machining), finish hand polishing, finish grit blasting, implant identification marking and cleaning and passivation processing [15]. Focusing our attention on titanium alloys, it is worth mentioning that they can be cast, rolled, forged and produced in a variety of mill products. Structures can be built by welding, brazing or adhesive bonding, reminding us that properties can be controlled by chemistry and processing [7]. Now that we have mentioned some traditional manufacturing processes, it is time to point out the innovative manufacturing procedure utilized for this study: Electron Beam Melting (EBM). Rapid manufacturing (RM) refers to the building process of a computer aided design (CAD) out of

Ti-6Al-4V powder by melting specific areas in a layer by layer fashion. Electron Beam Melting consists of focusing a high speed stream of electrons on a tiny spot aided by an electric field. This beam of electrons can be focused and/or bent by electrostatic and electromagnetic fields to melt the powder in contact. This process is driven by a computer system containing the component to be built [16]. EBM technology, which is in vacuum, can control ingot macrostructure by controlling the solidification conditions. This can be accomplished by utilizing electron-beam heating sources that can be independently controlled, which can provide a decent surface quality as compared to casting methods [17].

Just to mention a simple example, one of the main applications of Ti-6Al-4V is for biomedical implants, such as hip implants. According to Lutjering, to increase bone ingrowth the roughness of the stem surface has to be increased, facilitating bioadhesion. The common manufacturing methods used for hip stems are forging and investment casting. The advantage of investment casting is that surface roughness can be obtained directly, but the fatigue strength of investment casting with no heat treatment performed is usually less than for forged titanium [8]. By EBM manufacturing, the creation of hip implants with the required roughness can easily be achieved in a single step with no heat treatments necessary to obtain the fatigue strength of a forged alloy.

CHAPTER 3

METHODOLOGY

3.1 Specimen's Creation

In order to initiate the study, several components were designed in SolidWorks™ and Materialize/Magic™ softwares. These components varied in dimensions, shapes and densities. To provide a simple example, initial specimens were 1cm cubes followed by cylinders of 2cm in diameter and 10cm long that were later used to create tensile specimens. It is important to mention that these components were of different densities, starting with fully solid components of a density of 4.9g/cm^3 and continuing with mesh and foam components of lower densities, being this is a major key to create bone compatible structures. Once the components were designed, they were created by rapid prototyping using an electron beam melting machine: ARCAM A2.

3.2 Electron Beam Melting

High precision and quality can be obtained out of the ARCAM A2 machine used for this study. EBM rapid prototyping makes possible the creation of a metal complex component out of a computer design model by melting powder particles. This process is ideal for high strength or high temperature applications, since the powder material used is Ti-6Al-4V and/or Ti-6Al-4V ELI besides the advantage of being a low density alloy [18].

The EBM system shown in figure 3.2.1 has an operation system similar to an optical or electron beam welding system. It utilizes a current of ~10A (DC) that drives a tungsten filament in the electron gun operating at an anode potential of 60 kV, shown by number 1.

Number 2 shows a set of electromagnetic lenses used to focus the electron beam along with the aid of scanning coils located at number 3. Number 4 shows two powder cassettes located at each side of the system that feed the building table at 7 by providing a uniform layer of Ti-6Al-4V powder raked by number 5 to create the designed component into a solid form in the building chamber at 6. The build chamber works under a vacuum of $\sim 10^{-4}$ Torr and normal building utilizes a helium gas bleed at $\sim 10^{-2}$ Torr to facilitate build cooling and thermal stability. The melt scan is driven by a three dimensional (3D) computer aided design (CAD) program melting only the desired portions in the powder layer. Before melting the powder the system scans the beam eleven times to preheat the layer at an approximate velocity of 15,000mm/s and then a melt scan at 400mm/s is provided. The temperature is maintained at ~650°C throughout the entire process [19,20].

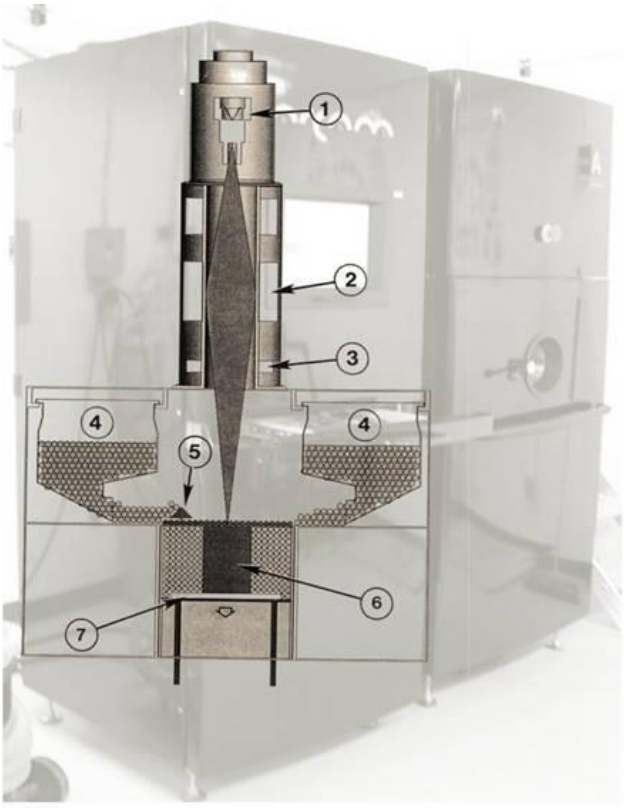

Figure 3.2.1 Arcam A2 system with schematic showing the inside of the machine.

3.3 Optical Metallography

Microstructural analysis was performed on horizontal and vertical cross sections of the EBM specimens. An optical microscope Reichert MEF4 A/M was utilized after cold-mounting, grinding up to 1200 grit and a final polish of 0.05μm alumina paste on specific areas of the component. Then, the mirror-like finished samples were etched with a solution consisting of 100 mL H_20, 2.5 mL HF, and 5 mL HNO_3 and then rinsed in ethanol for analysis purposes.

3.4 Scanning Electron Microscopy

A Hitachi S4800 field-emission SEM utilizing secondary electron imaging at an accelerating voltage of 20kV was used to inspect the components created in the ARCAM system as well as the Ti-6Al-4V powder utilized at different stages of the building process. Energy Dispersive X-ray Spectroscopy (EDAX) was used to perform a chemical analysis of the powder particles used in the EBM process as well.

3.5 Hardness and Tensile Testing

Hardness testing was performed with either 25 and/or 100 grams load in a Shimadzu HMV-2000 microindentation tester. Rockwell C-scale hardness (HRC) with a load of 150 kgf (1.5 kN) was performed on EBM samples before and after HIPing. HIPing consisted in placing cylindrical (~2cm in diameter and ~15 cm long) samples under a force of 0.1GPa at 900°C for two hours. Tensile testing for solid, fully dense cylindrical components was performed in an Instron 500R tensile machine using special grips at an engineering strain rate of 3×10^{-3} s^{-1} at room temperature (20°C). Additionally, fracture

surface analysis was performed in the scanning electron microscope. Tensile testing was used to obtain yield strength, ultimate tensile strength and percent elongation in EBM samples before and after HIPing for comparison purposes.

3.6 Transmission Electron Microscopy

Different samples were thinned to a thickness less than 0.2mm and then punched into 3mm diameter disks. Electrojet polish was performed using a Struers Tenupol-5 dual-jet unit using a solution consisting of 0.9L of methanol and 50mL of H_2SO_4 at a temperature of -15°C and using a voltage of 13V for most of the samples. The shiny (hole induced) samples obtained from the polisher were examined in a Hitachi H-8000 analytical Transmission Electron Microscope (TEM) at 200kV accelerating potential, utilizing a goniometer-tilt stage and a Hitachi H-9500 TEM at 300kV was utilized only to obtain images.

CHAPTER 4

RESULTS AND DISCUSSION

4.1 Ti-6Al-4V Powder Analysis and Recycling

One way of producing Ti-6Al-4V powder is by gas atomization, which consists of the disintegration of molten metal into powder by using high pressure gas in a closed, inert gas-filled chamber to prevent contamination. Spherical particles are obtained by the expanding gas breaking the melt stream into molten droplets that spheroidize before reaching solidification. Higher melt temperatures and gas pressures are used to obtain smaller particles, figure 4.1.1 shows a schematic of this procedure [8,21].

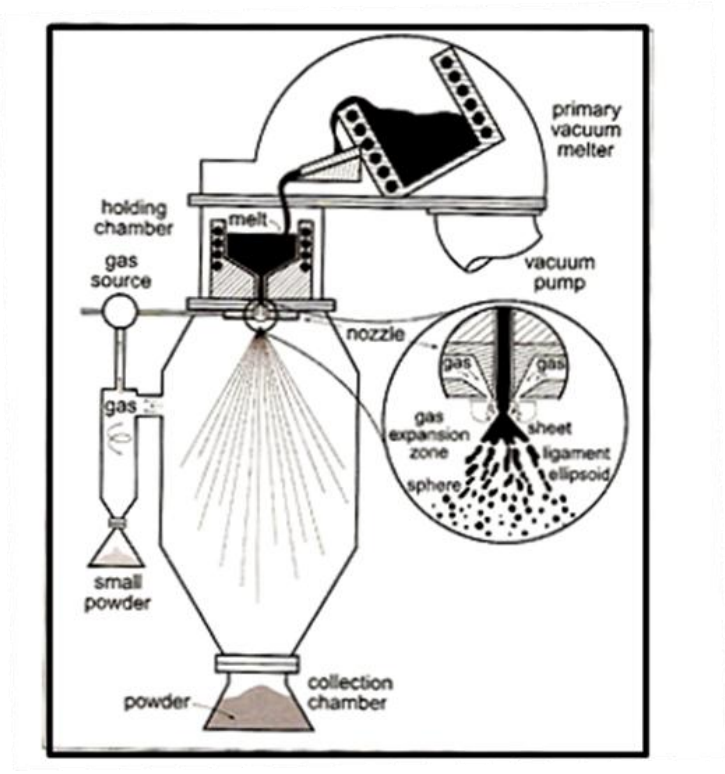

Figure 4.1.1 Gas atomization process

Since there is some concern about an alteration that some aluminum content can be lost during the EBM layered manufacturing, Ti-6Al-4V powder was chemically analyzed to obtain a further understanding of the alloy behavior. Energy Dispersive X-ray Spectrometry (EDS), in the FESEM with an elemental quantitative accuracy of ~1 weight per cent, was used to examine different types of powders by analyzing the aluminum and vanadium content. The different powders consisted in original or new powder; breakaway powder, which is the powder that can be easily removed from the EBM builds, and breakaway powder after 10 cycles of use. Another type of powder analyzed is the recovered powder from the build table after one cycle and the same after 10 cycles of use. In addition, the prep powder which is the mixture of the starting, the recovered, and the breakaway powder and finally the recycled powder, which is the one being sifted after being detached from the built components at the build table, no starting powder added.

While the recycled powder showed a higher weight percentage of vanadium, all the powders were presumably equal in aluminum content. It can be seen that figure 4.1.2 shows the different percentages in aluminum and vanadium for the different types of powder. It can also be highlighted that no decline in the aluminum content of the recycled powder is observed. While the theoretical total weight percentage for aluminum and vanadium in the Ti-6Al-4V should be 10%, it ranged from 9.7% to 10.3% without taking into consideration the recycled powder that had a total of 11.5% weight percent, mainly due to the increase in vanadium content. For each type of powder, eleven measurements of single powder particles at two different magnifications were analyzed in the EDAX/SEM.

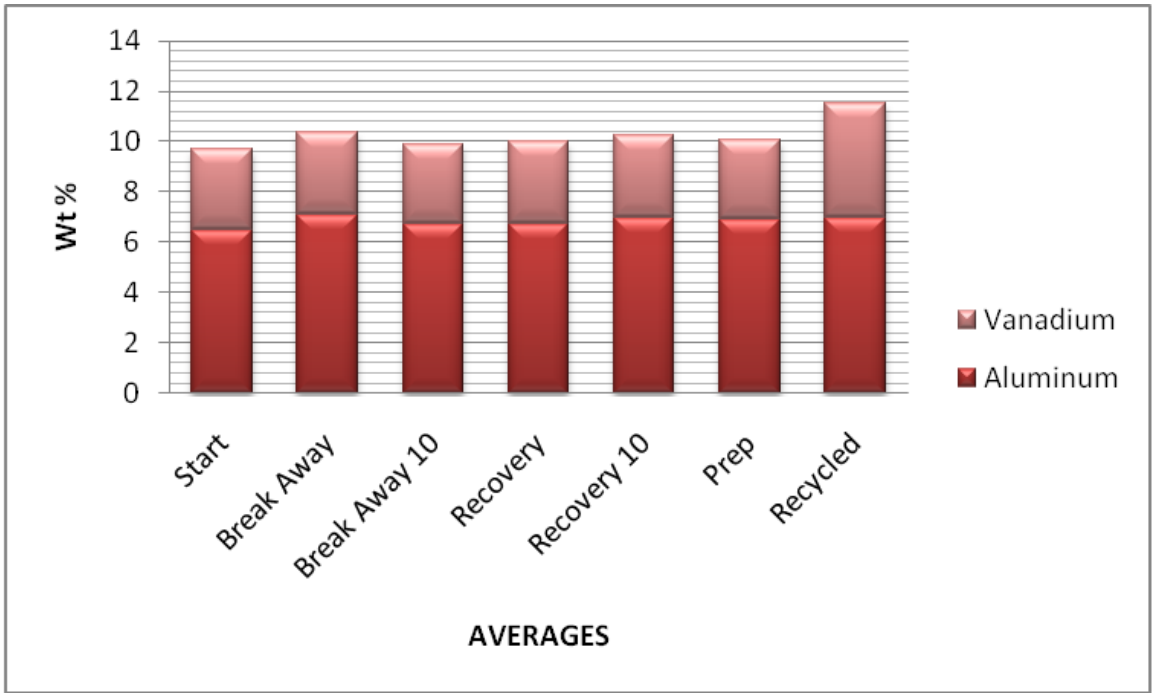

Figure 4.1.2 Weight percent of different powders analyzed

Besides analyzing the aluminum content in different powder particles, a size distribution of the recycled powder particles was performed by using scanning electron micrographs of the same. Figure 4.1.3 shows an SEM image depicting the particle size distribution for the recycled powder utilized, among others, for the histogram creation. Some powder agglomerations can also be observed from the picture. It should be mentioned that no irregular-shaped particles were taken into consideration for the histogram creation. From figure 4.1.4 it can be seen that particles varied in size, ranging from 3 to 100μm, showing an average of 46μm but having the mode in between 50 to 59μm. A bimodal distribution can be observed from the histogram, showing a small particle size average of 17μm and a large particle size average of 59μm.

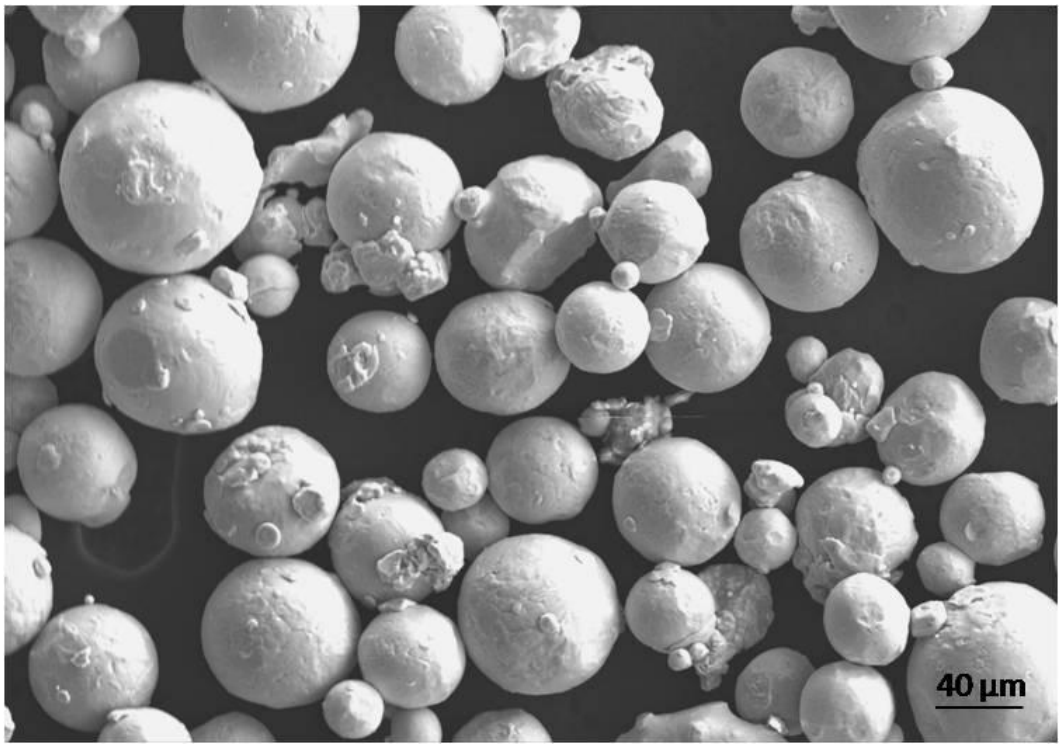

Figure 4.1.3 SEM micrograph showing particle size distribution in recycled powder.

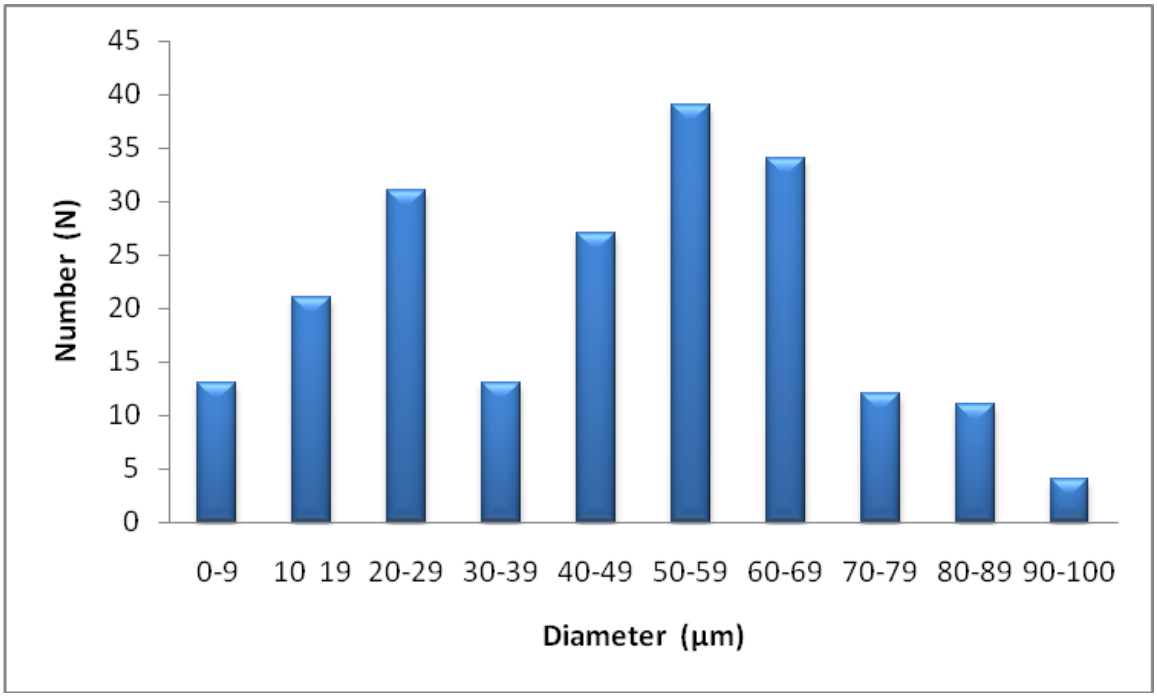

Figure 4.1.4 Particle size distribution of recycled powder

4.2 EBM Parameters

As mentioned before at the beginning of this study, different parameters were analyzed in order to obtain the best microstructural characteristics of the build. When the parameters of the system are not properly optimized this can create large amounts of build defects. Another reason for the appearance of these defects could be that the beam is being interrupted or that the addition of impurities in the system could be creating beam tripping. One example of this is shown in the SEM micrographs in figure 4.2.1a, where a continuous beam tripping can be appreciated in the top portion of the build. Figure 4.2.1b shows a higher magnification of a particular portion of the defect next to spherical voids in the build.

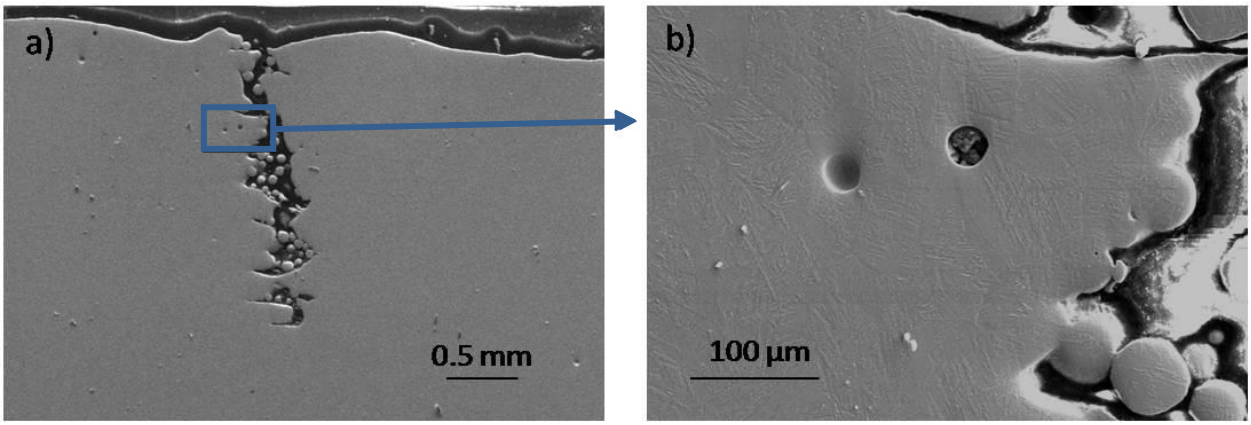

Figure 4.2.1 Example of beam tripping (a) and the magnified view of marked area (b).

Irregular shaped voids were found in 1x1x1 cm cubes built by the EBM system before changing the parameters of the system. These builds were completely ground and etched from top to bottom and optical microscopy was performed on a digital imaging Reichert MEF4 A/M system was used to check if what seemed to be an imperfection was

actually a void. After using the optical microscope, the next step was to run the sample in the Hitachi S-4800 scanning electron microscope to document the different voids or related defects found in the small cubes. Figure 4.2.2 shows an optical micrograph of an irregular void found in one of the cubes. Additionally, figure 4.2.3 shows the same irregular imperfection from figure 4.2.2 observed in the SEM, showing non-melted particles inside it. It can be seen that the optical micrograph shows some metal inside the void as well as spherical shiny areas, see the arrows in the micrograph, while the SEM micrograph shows complete non-melted particles inside the void where at the location of the shiny areas. Take into consideration that both micrographs show the same sample at the same area but inverted since they were taken by two different microscopes. Figure 4.2.4 shows more examples of irregular-shape imperfections found in the components before EBM parameters were optimized, while figure 4.2.5 shows a soon-to-become a void, if ground more it would show a bigger void area.

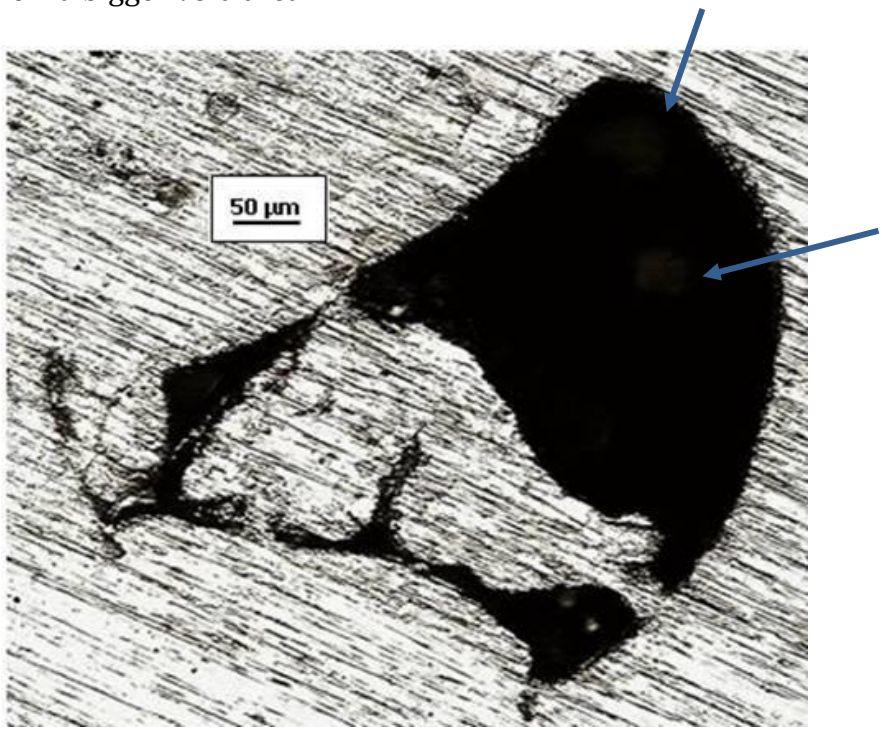

Figure 4.2.2.Optical micrograph showing an irregular imperfection in EBM built

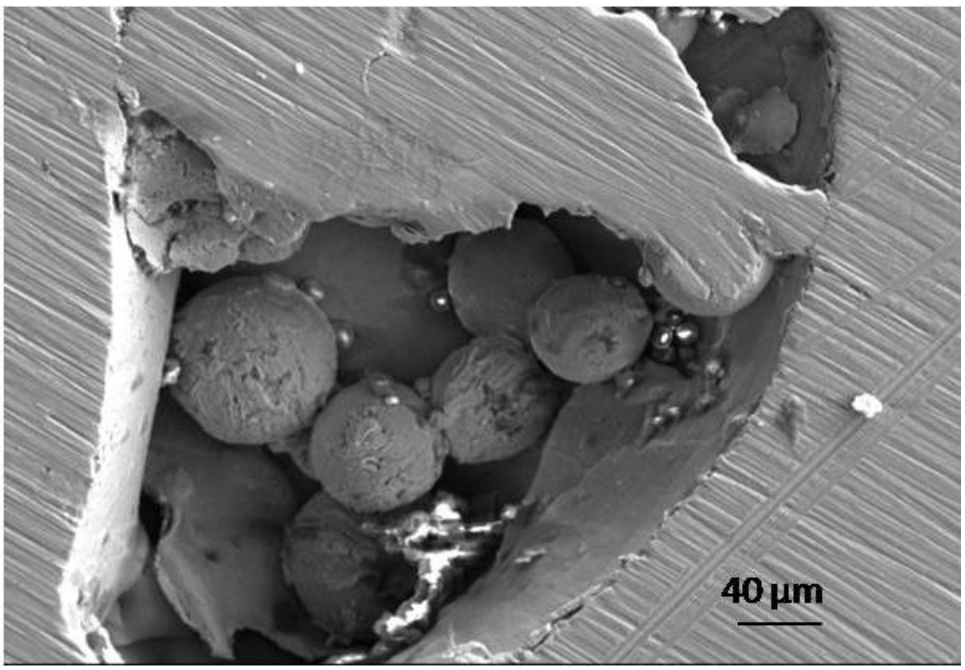

Figure 4.2.3. SEM micrograph showing imperfection in the EBM builts from figure 4.3.2

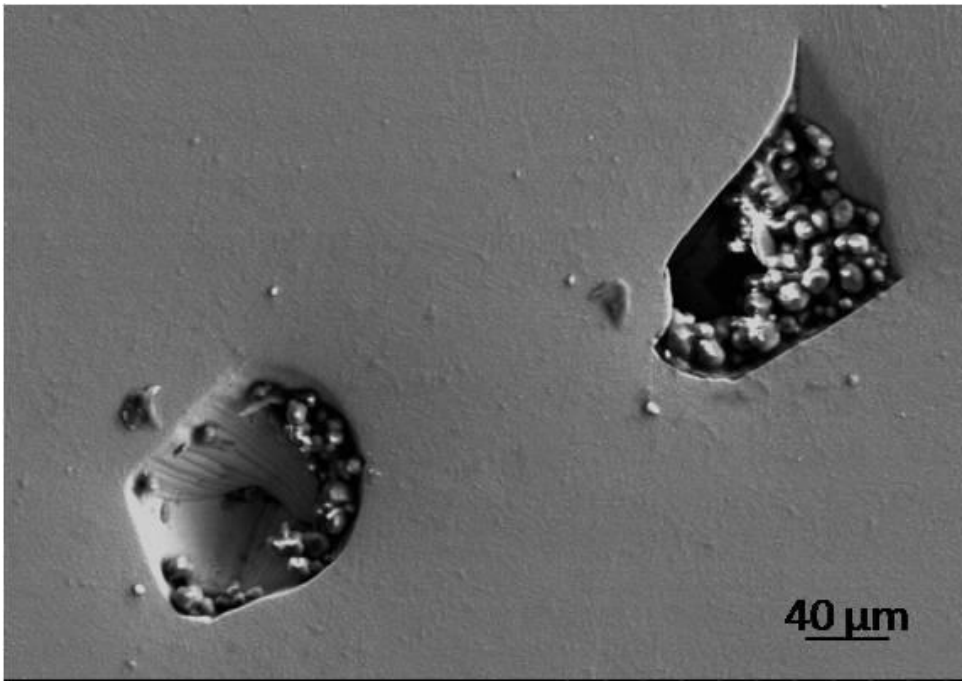

Figure 4.2.4 Irregular-shape imperfections shown in SEM image

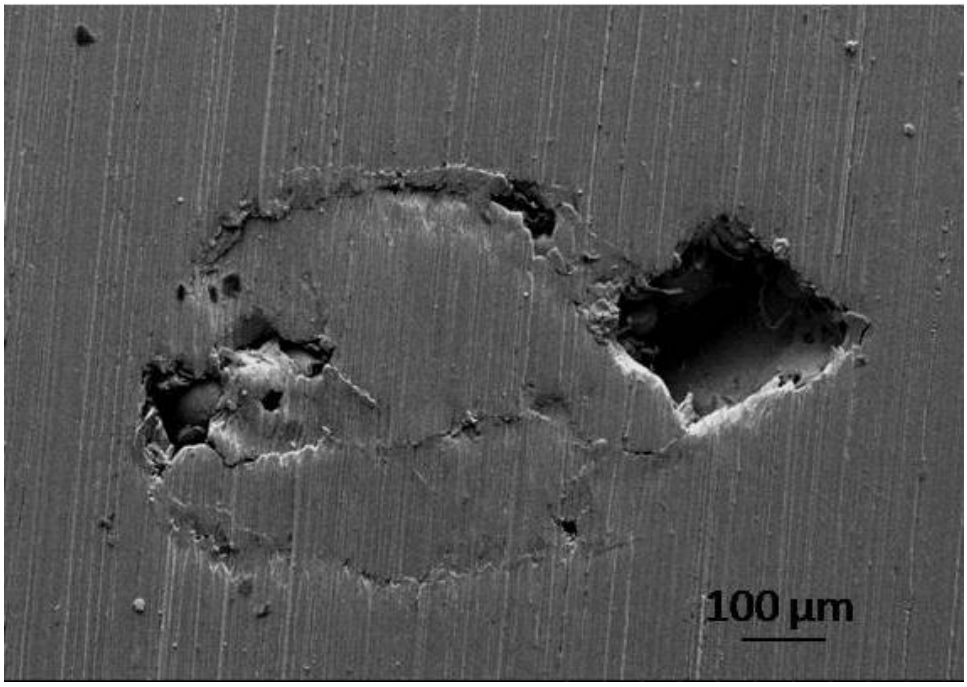

Figure 4.2.5 Imperfection shown in SEM image where if grinded more a bigger void will appear

Lens current and beam scan speed were the first parameters changed, ranging from 4 to 7 mA for current and 200 to 600 mm/s for scanning speed, using an arbitrary focus of 26. For a focus of 30, a set of builds were created with the current varying from 1 to 10 mA, and a scanning speed varying from 100 to 1000 mm/s. As a result, it was found that the setting with the least visible imperfections were 6mA, 400mm/s and a focus of 30, shown in figure 4.2.6. Figure 4.2.6 also shows one more set of parameter combinations while figure 4.2.7 shows two more that created high porosity zones in the built components. Various densities obtained from the different parameters due to the non-melted particles in the components can be observed, considering the specimens had exactly the same dimensions. They vary from 2.83 (0.64ρ) to 4.43 g/cm^3 being the last one fabricated at the optimized parameters: 6mA and 400mm/s. It can also be appreciated how having the

wrong parameters provides undesired non-melted particles throughout the build. The photograph next to each cube in figure 4.2.6 and 4.2.7 represents the top face of the 1x1cm^2 built showing the differences in porosity on the surface before any grinding and polishing was performed on the samples.

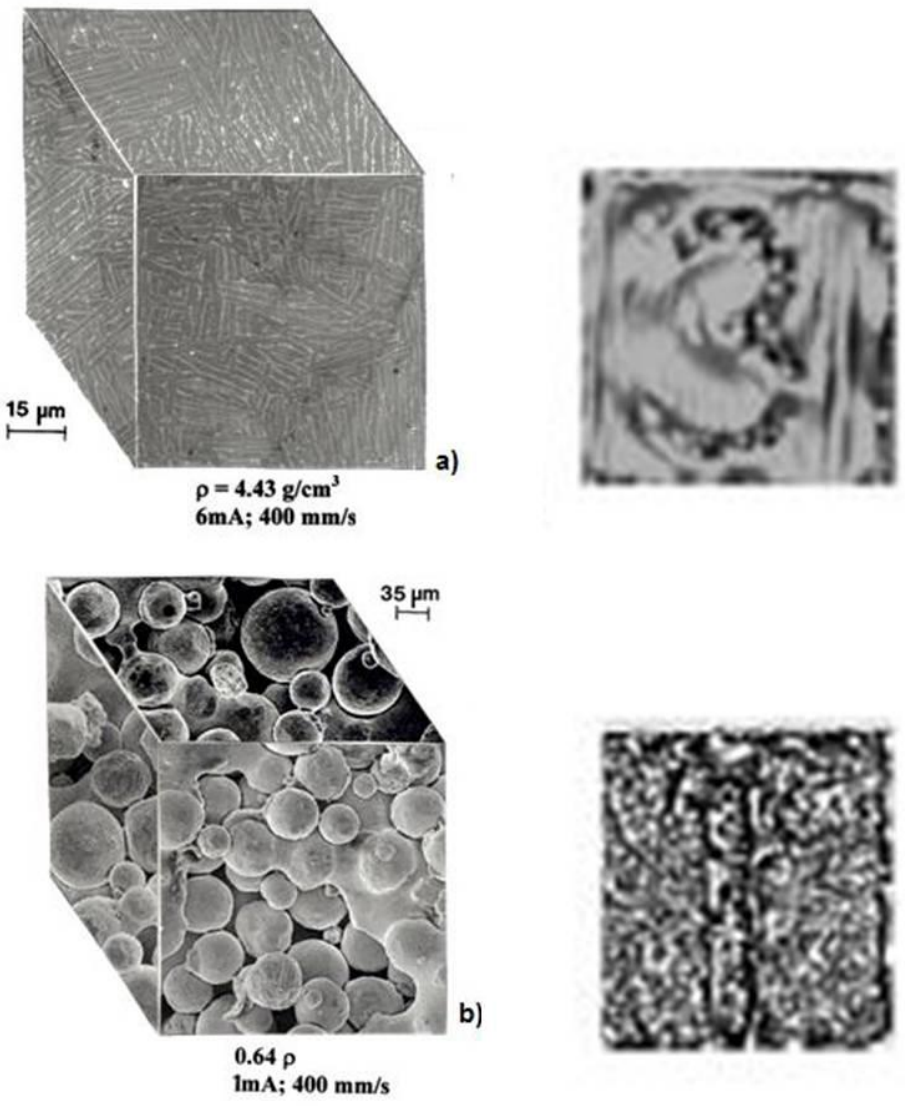

Figure 4.2.6 Current and scanning speed analyzed at a focus of 30 and 400 mm/s for 6 and 1 mA

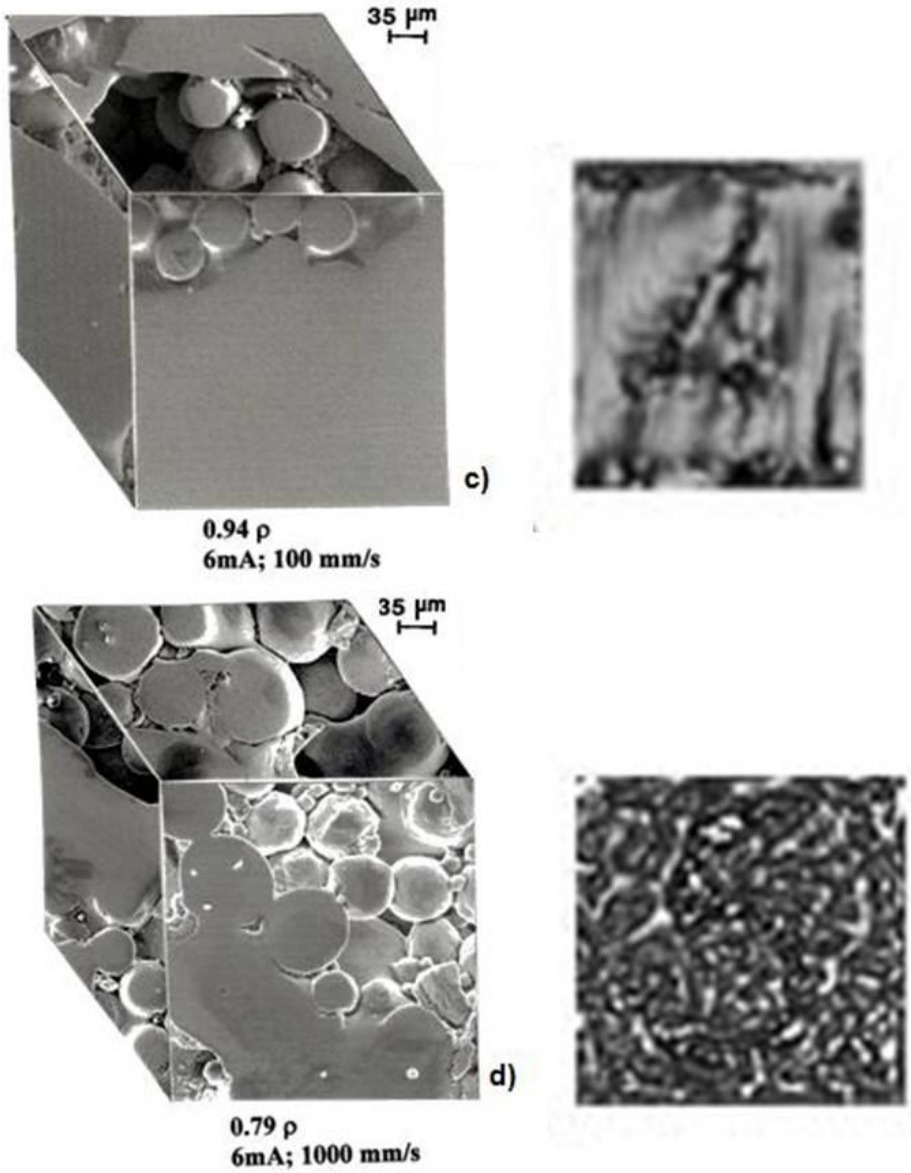

Figure 4.2.7 Current and scanning speed analyzed at a focus of 30 and 6mA for 100 and 1000mm/s

4.3 Specimens Created

As already mentioned the first set of samples consisted of ten specimens fabricated with a focus of 26 and lens current varying from 4 to 7 mA and a beam scan speed ranging from 200 to 600 mm/s. The specimen's dimensions were 1x1x2 cm as observed in figure 4.3.1. Optical microscopy, Rockwell C-scale hardness and further analysis in the scanning electron microscope were performed to the samples named 1, 3, 5, 6 and 10 with a similar hardness ranging from 53 to 56 HRC.

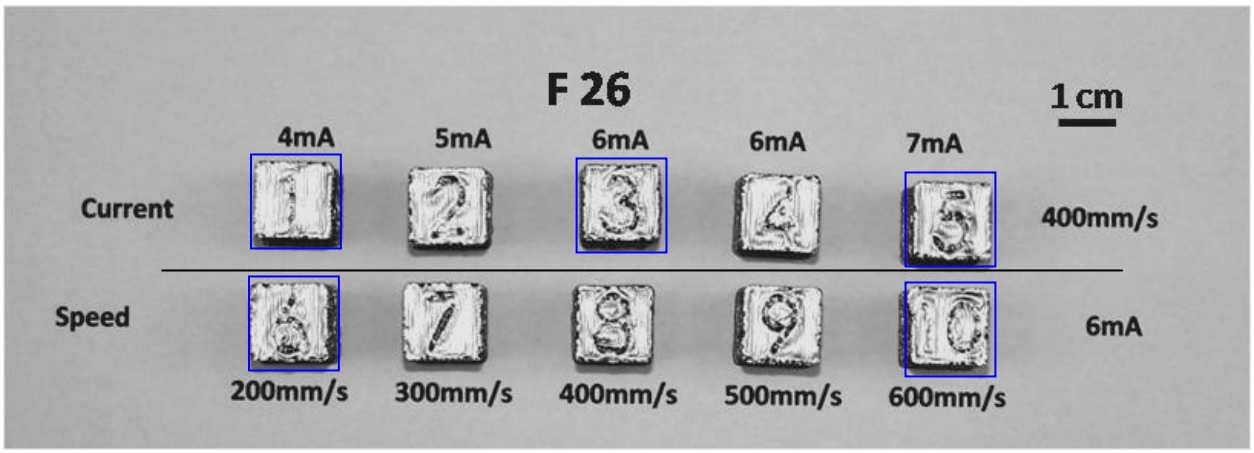

Figure 4.3.1 Set of EBM specimens with a focus of 26

The next set of components consisted of cubes of the same dimensions, this time only 5 cubes, with a focus of 30 and a wider range in current and speed. These cubes are shown in figure 4.3.2. Besides analyzing porosity, the density was measured by submerging the specimens in graduating cylinders and obtaining the weight from a precision weight, Sartorius MC 210S. Figure 4.3.2 shows the cubes as obtained from the EBM system. From both sets of cubes at focus 26 and 30, and the parameter combinations used in each cube, an adequate estimate of the standard parameters for the EBM system was decided. The

next parameters that were used for subsequent components was a focus of 30, a current lens of 6 mA and a beam scan speed of 400 mm/s, when the recommended parameters from the system manufacturers was a current of 6 mA, a scan speed of 400 mm/s, and a focus of 26.

Figure 4.3.2 Set of EBM specimens with a focus of 30

Once the optimum parameters were set for the system, specimens in cylinder-shape were also manufactured for metallography inspection, as well as hardness and tensile testing. The first two cylinders created were larger than the others (see figure 4.3.3) with an approximate diameter of 1.5 cm and 18 cm in length. These two cylinders were HIPed and a porosity analysis was performed, while the smaller cylinders were profoundly analyzed. The smaller cylinders, that we will refer to as standard size, have a diameter of 2 cm and an approximate length of 7cm. As already mentioned, different densities were achieved by changing the parameters in the system, since most of the time the beam did not have the current or the time necessary to melt every powder particle. Another way of creating components of various densities is by providing them open structures. An

example of the open structures used for the components is seen in figure 4.3.4; nevertheless, no analysis was performed to the component shown.

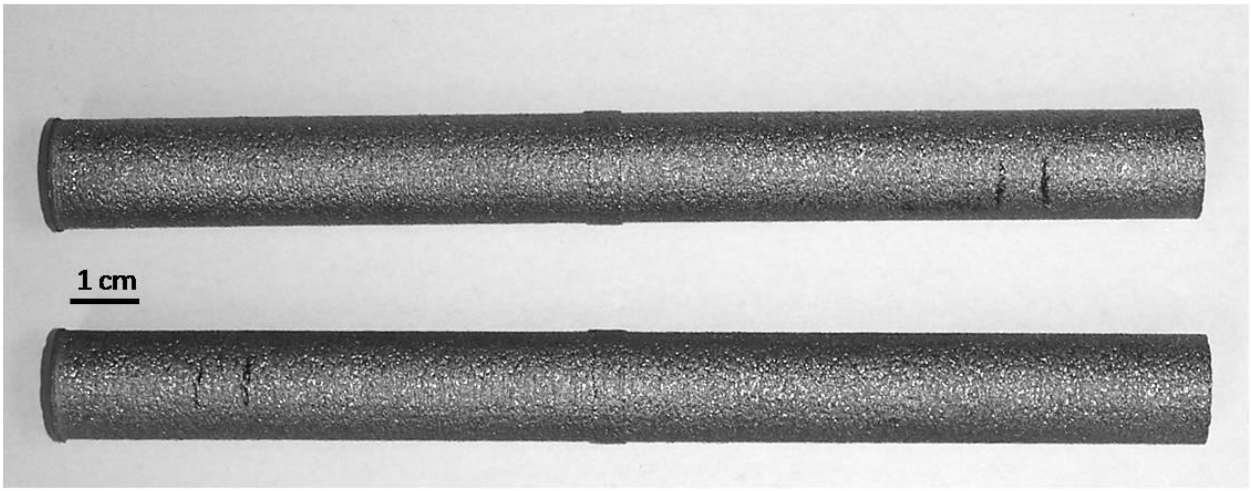

Figure 4.3.3 Cylinders used for HIP and porosity analysis

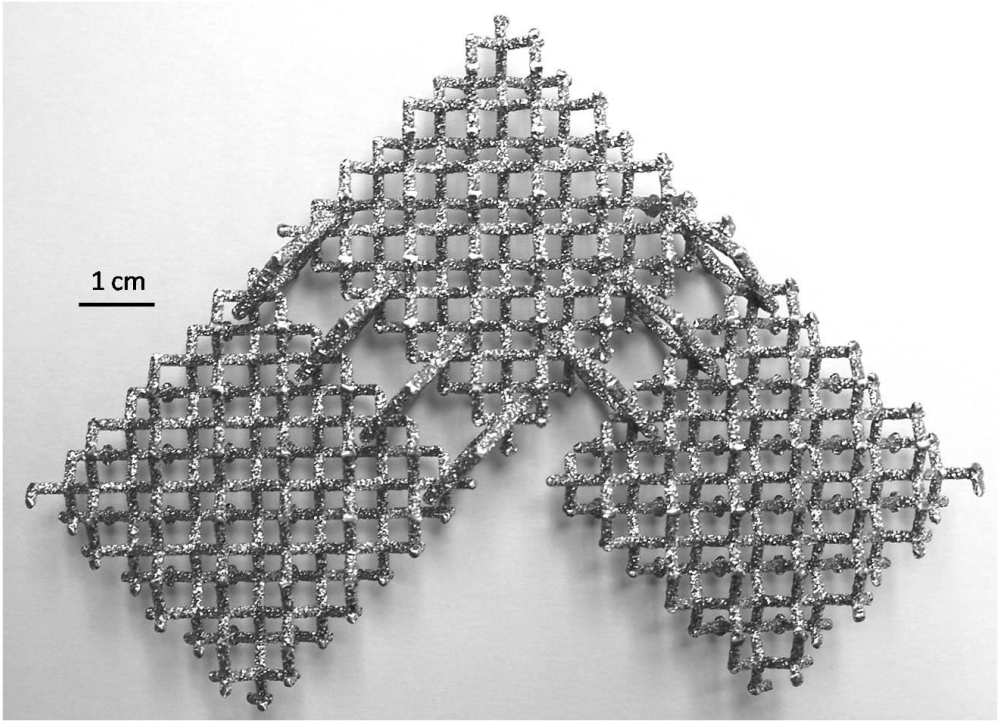

Figure 4.3.4 Open structure in a Ti-6Al-4V component

A Computer Axial Tomography (CT) scan was performed on aluminum foam and a basic unit was obtained and utilized to create Ti-6Al-4V foams of different densities that, if desired, can simulate the density of a bone. Different applications can be given to commercially available metal foams such as absorbing systems, filters, silencers, flow heat exchangers, etc. [22]. Figure 4.3.5 shows three different components, created from the aluminum scan, that have exactly the same dimension but having different densities. Notice how the foam-opening size decreases from left to right. After analyzing foam components, different geometrical structures were used to create the following components, referred to as mesh components. One example of this is the one shown in figure 4.3.6 where the basic geometrical unit is a three dimensional cross.

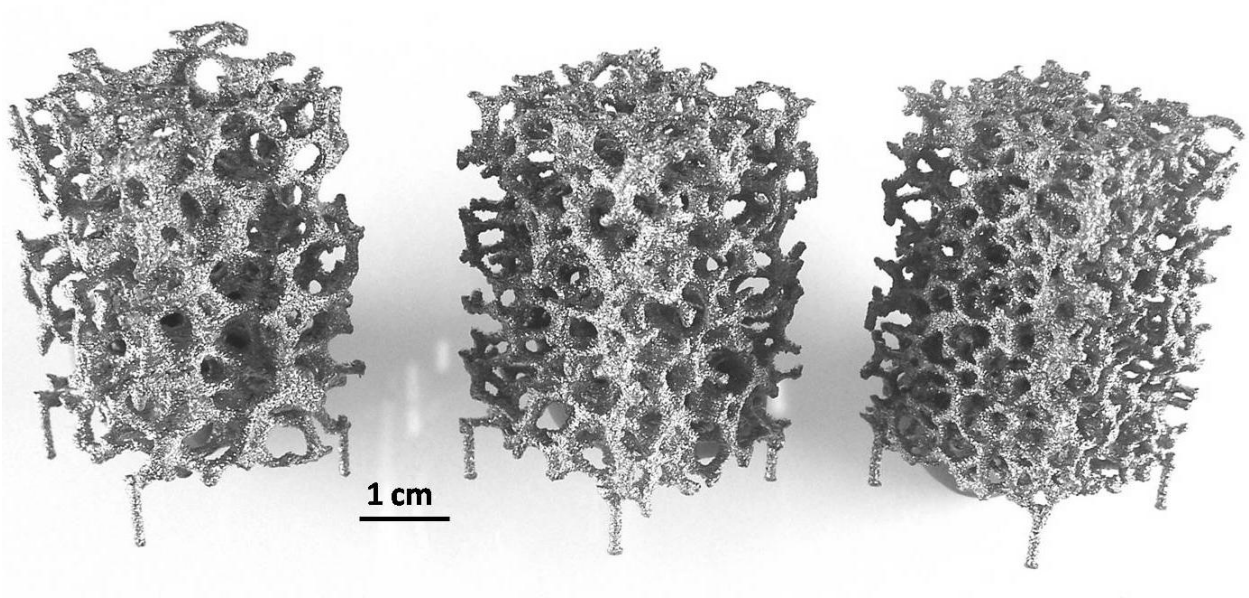

Figure 4.3.5 EBM-manufactured components obtained out of an aluminum CT scan

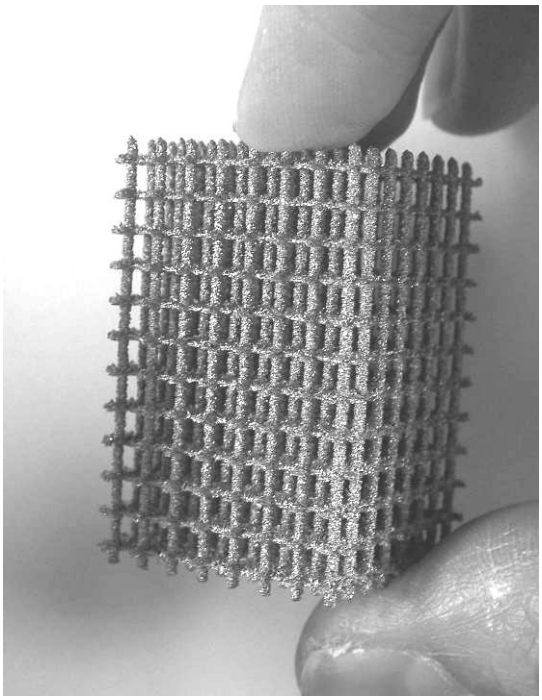

Figure 4.3.6 Example of one of the mesh components fabricated by EBM

In addition, mesh components were built out of more geometrical mesh arrays as shown in figure 4.3.7, including the cross geometry already shown. These components were fabricated from different software build elements such as dode-thin, G7, G6, 7r and cross 1, from Materialise™. The structure indicated as 7r is seen from a different angle of the G7 geometry. Moreover, G7 geometry can be thought as a more complex geometry variation of G6. Corresponding low magnification SEM images of the strut structures already mentioned are also shown in figure 4.3.7. In accordance, the density for the mesh can be varied by changing the size of the elements.

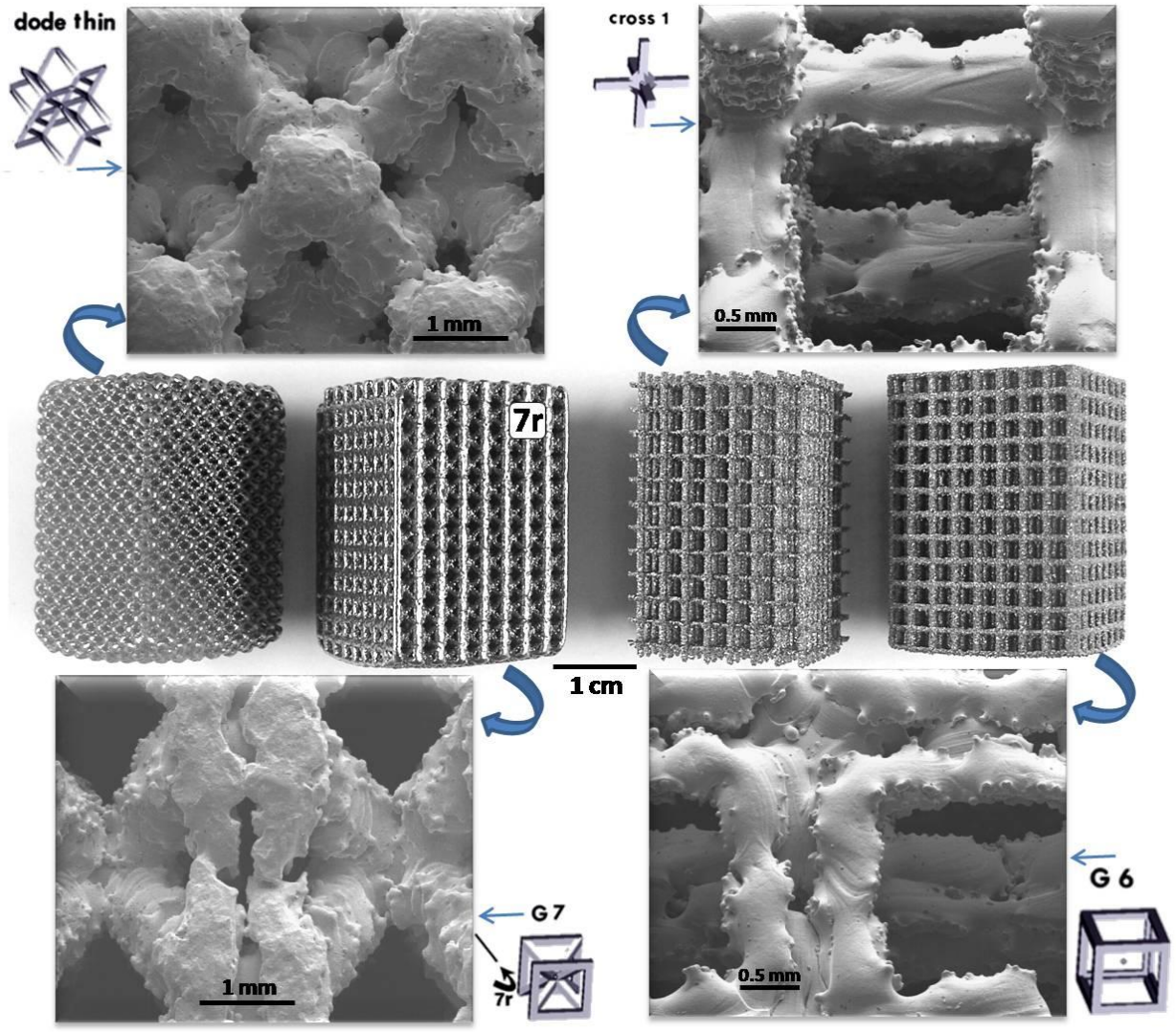

Figure 4.3.7 Fabricated mesh blocks with their corresponding strut SEM image and CAD model structure generators

4.4 Ti-6Al-4V Porosity

Spherical voids existed before the EBM system created the samples. The reason why is because argon gas was trapped in the atomized powder as a gas bubble during the rapid solidification process. Powder particles were analyzed by optical and scanning electron microscopy and spherical voids were observed in single particles which lead us to

the conclusion that gas was already trapped in the powders from the gas atomization process. Figure 4.4.1 and 4.4.2 show gas voids in Ti-6Al-4V start powder taken in the scanning electron microscope. Figure 4.4.1 shows how powder particles that have not gone through the electron beam melting process show porosity and how much smaller particles can fit the pore. This might be one of many indications that void powder particles are completely hollow on the inside. Figure 4.4.2 shows a different start powder particles showing porosity.

Figure 4.4.3 shows a SEM image of the prep powder, which is the mixture of start, recovered and break away powder, showing porosity. Since the powder particles were mixed with liquid Koldmount and left to dry in a one-inch diameter container, it can be observed how over-charging was affecting the image quality. SEM voltage had to be lowered to ~8kV from 20kV usually used. Figure 4.4.4 shows a light optical microscope image showing a different prep powder particle with porosity on the cross section. Microstructure can be appreciated from the micrograph taken in the optical microscope since it was ground, polished and etched, as regular solid components. Cross sectional images of the voids, besides showing microstructural features, can demonstrate that gas bubbles trapped in the powder particles do not necessarily occupy the whole area inside the particle, they randomly vary in size.

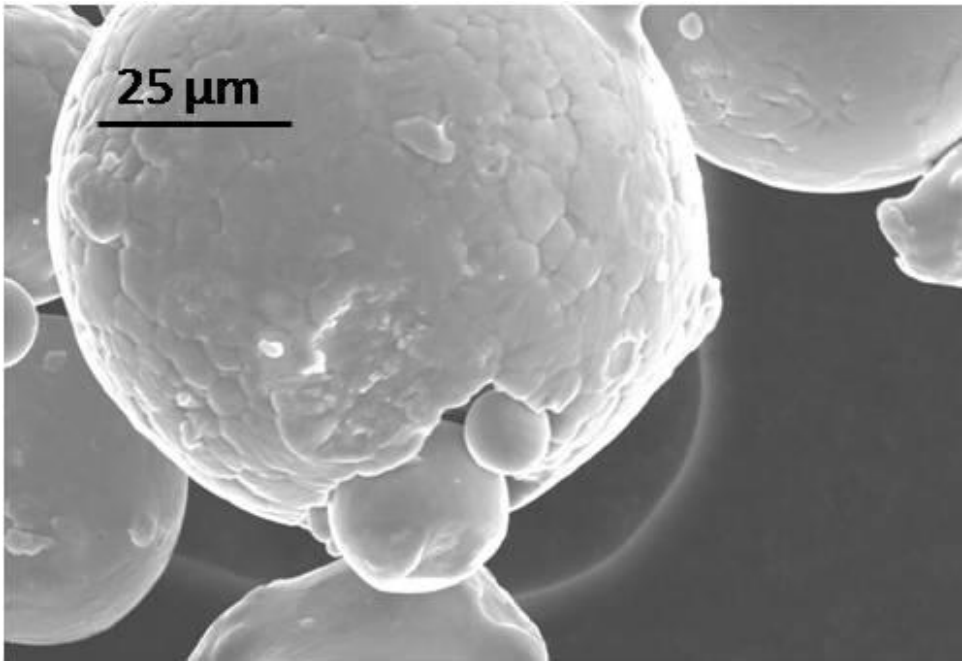

Figure 4.4.1 SEM micrographs of start powder particles

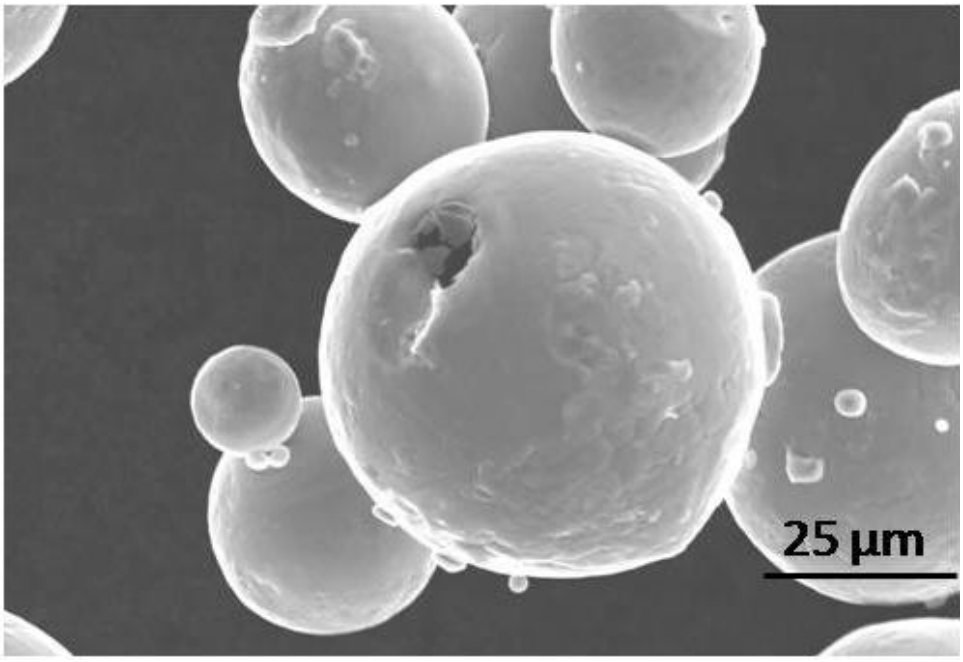

Figure 4.4.2 SEM micrograph of start powder particles showing porosity

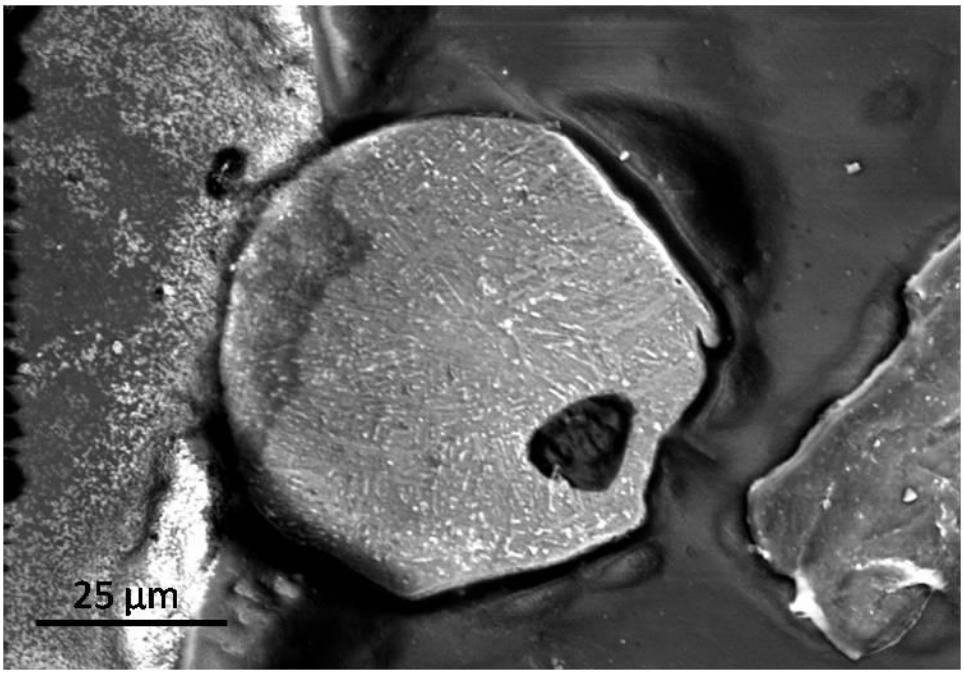

Figure 4.4.3 SEM micrograph of prep powder particles showing porosity

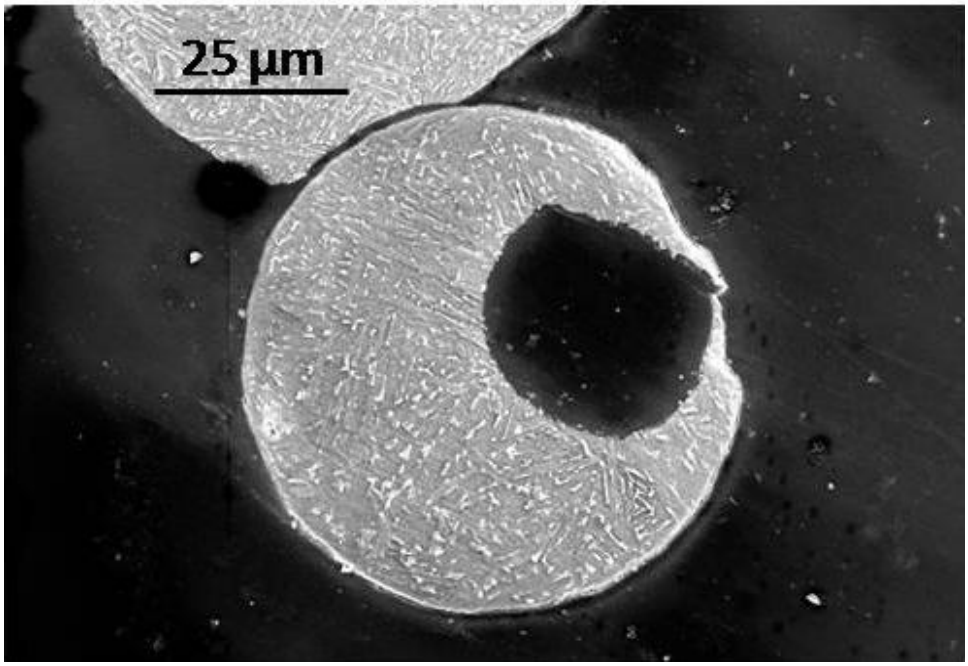

Figure 4.4.4 Prep powder micrograph showing porosity in LOM

As mentioned before, several were the samples obtained out of the EBM system. After obtaining the standard parameters for the system it was found that spherical voids were still persisting in the samples. According to Lütjering and Williams, when forgings made from a billet are created using a rotary general forging machine and the critical strain for ductile fracture is exceeded small voids are formed, known as strain induced porosity. Once these voids are created in a forging billet they will not always be healed by subsequent forging operations. These voids can be a defect that will act as an early fatigue crack initiation site [8]. Figure 4.4.5 shows the same defect obtained from the prep powder in both LOM and SEM. This can be considered as the cross section of the powder particles, and it can be seen that the defects obtained from the powder, not necessarily the EBM system, are spherical in shape. The spheroid shape of the defects can be another indication of how gas atomization is the reason of these voids.

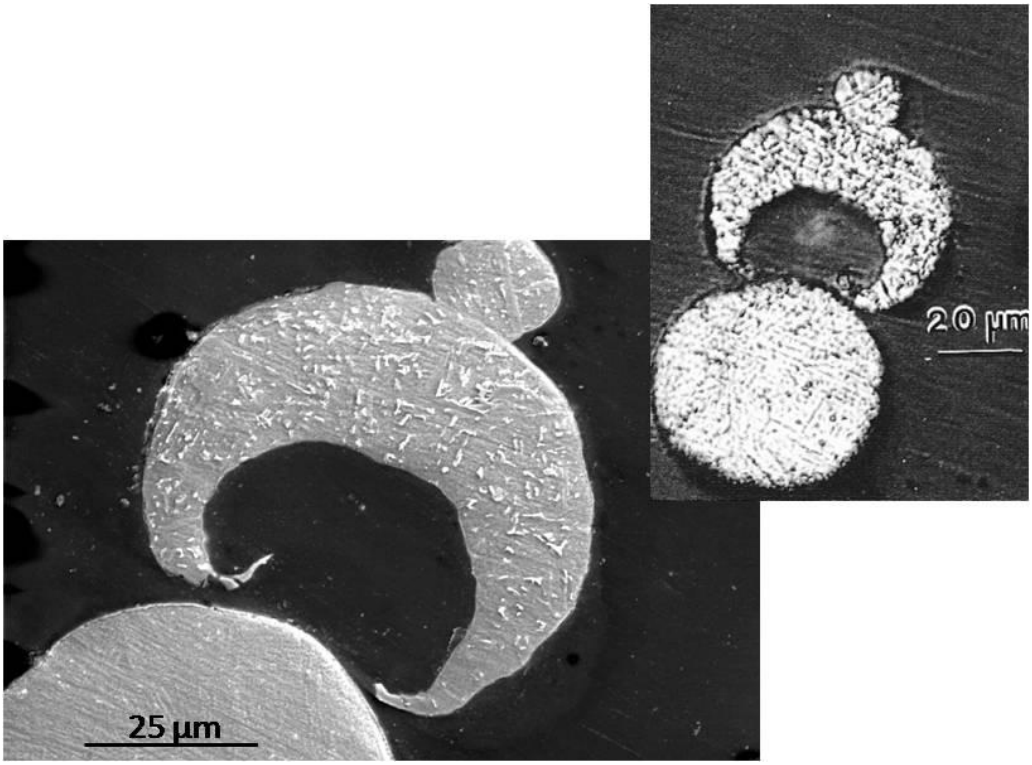

Figure 4.4.5 Cross section of prep powder showing spherical defect.

Every time new samples with different parameters were fabricated they were examined by optical microscopy. Even though several parameters were changed and optimized, at least one small void was found in the mirror-finish polished face of the sample. Figure 4.4.5 shows a scanning electron microscope image of a cut, ground, polished and etched sample with a spherical void of a size less than the average powder particle, ~45μm in diameter, while figure 4.4.6 shows an optical micrograph of two small voids found in a sample with the standard parameters (6mA, 400mm/s and a focus of 30), microstructural features can be appreciated in both micrographs.

Since hot isostatic pressing (HIP) is used to improve fatigue properties of titanium castings and to heal internal porosity [8]. For this study HIPing under a standard routine was performed to EBM builds at a temperature of 900°C at 0.1GPa pressure for two hours. Figure 4.4.7 shows an area where almost no defects can be noticeable while figure 4.4.8 shows a linear defect that can be interpreted as the closing feature remaining of an spherical void after HIPing. It was found out that even though the single HIP cycle could eliminate most of the voids some remnants still persisted as shown in the SEM micrographs in figure 4.4.7 and 4.4.8. Even though HIPing shows a nice and huge improvement in specimen's porosity it was not performed again in subsequent components for practical purposes since samples had to be sent away for the HIPing process.

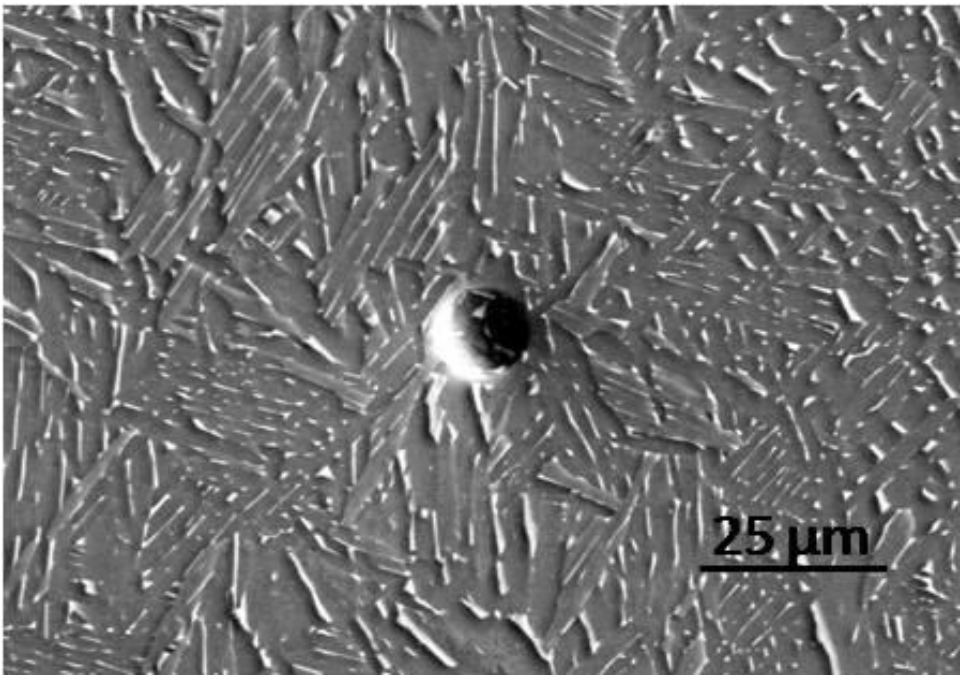

Figure 4.4.5 Spherical defect in SEM image of component built with standard parameters

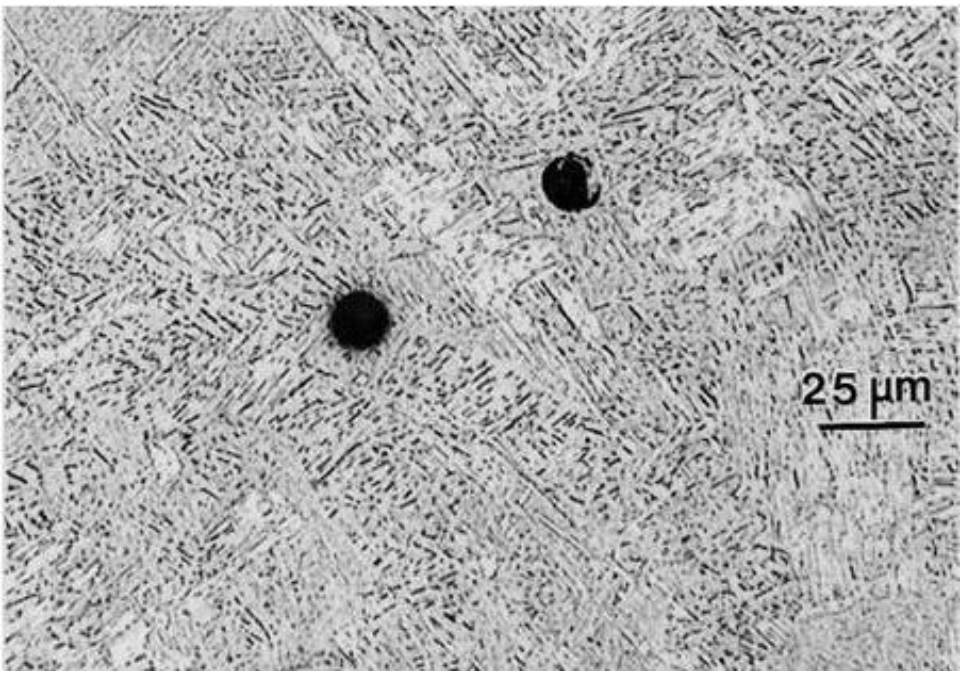

Figure 4.4.6 Spherical defects image of LOM of component built with standard parameters

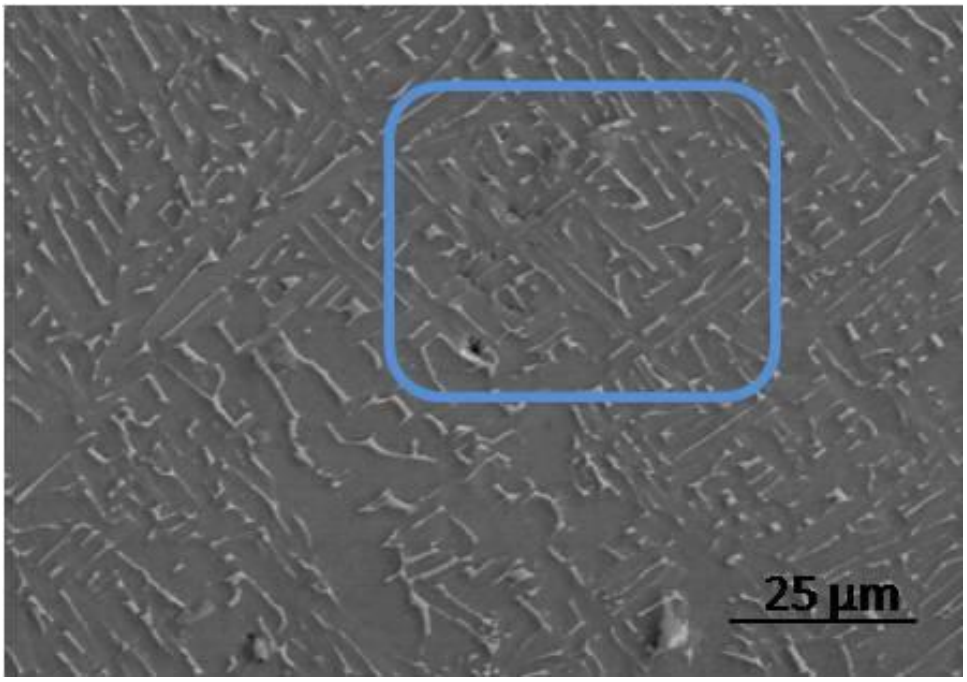

Figure 4.4.7 HIPed components

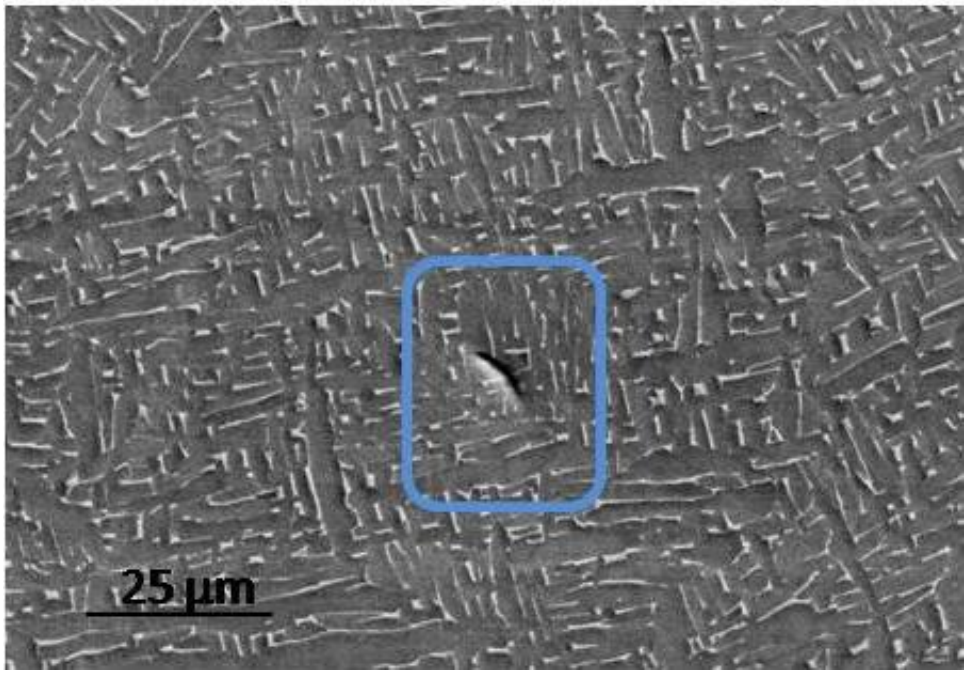

Figure 4.4.8 HIPed components

4.5 Microstructure

Being Ti-6Al-4V an α-β alloy, it is stated how microstructure varies based on thermal history at room temperature. A range of temperatures is given for solidification as liquid transforms to solid. Nucleation and growth characteristics of the alloy as well as the thermal conditions during solidification are responsible for grain size and morphology, and the crystallographic texture [23].

For this project, different Ti-6Al-4V components, after being cut, ground, polished and etched in an acidic solution consisting of 100mL of water, 2.5mL of hydrofluoric acid and 5mL of nitric acid, rinsed in water and air dried, were analyzed by optical microscopy. It is important to mention that several were the samples analyzed for this project. Cylinders fabricated by EBM Ti-6Al-4V were analyzed from both top and bottom approximately one centimeter from the edges. In addition, several were the mesh components analyzed consisting of different geometrical structures as shown in figure 4.3.7, providing similar microstructure for each sample. The same situation can be stated for the foam components. Foam samples differing in density, as shown in figure 4.3.5 (where the density of the components is increasing from left to right), where analyzed resulting in similar microstructural features. For practical purposes, only the most relevant micrographs are shown.

Figure 4.5.1 shows the component with the standard parameters 400mm/s and 6 mA for scan speed and lens current with an arbitrary focus of 26. This image shows the characteristic acicular α-phase structure with continuous interphase β. Figure 4.5.2 shows a similar microstructure for a component with a focus of 30, a scan speed of 400mm/s and lens current of 6mA. Since both micrographs were taken at the same magnification it can

easily be observed that the second micrograph, of a focus of 30, shows a more compacted structure compared to the micrograph taken for the component with a focus of 26.

Once the focus was set to 30, cylinders of the standard size, ~2cm in diameter and 7cm length, were cut, mounted and analyzed, cross section area of approximately 1cm from the top and 1cm from the bottom. Figure 4.5.3 and 4.5.4 illustrate micrographs at the same magnification showing top and bottom sections, respectively, of a cylindrical component that had two melt scan passes instead of only one. It can be observed that the top section shows a larger microstructure due to the difference in cooling rate. EBM cylinder components were built in a vertical axis from bottom to top, which provides a continuous heat to the previous layer, the one already built and shifted down 100μm. Considering that a new layer of powder at much lower temperatures is located on top of this layer, a "quenching-type" process occurs in the first layer build and therefore a martensitic-structure is observed.

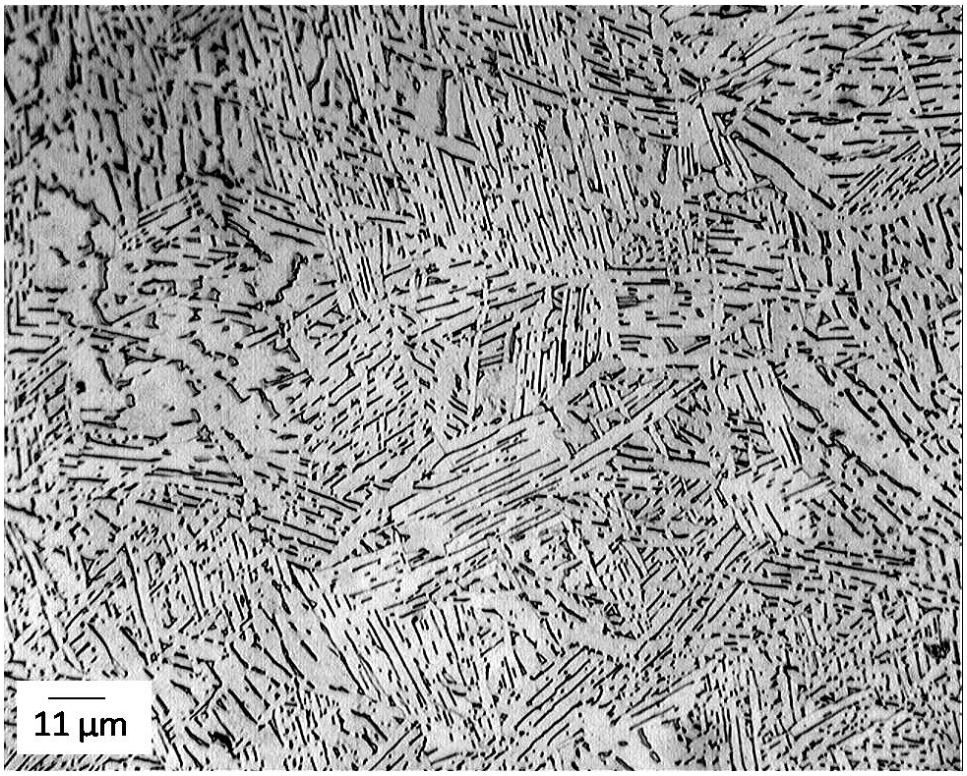

Figure 4.5.1 EBM component: Focus 26, 400mm/s and 6mA

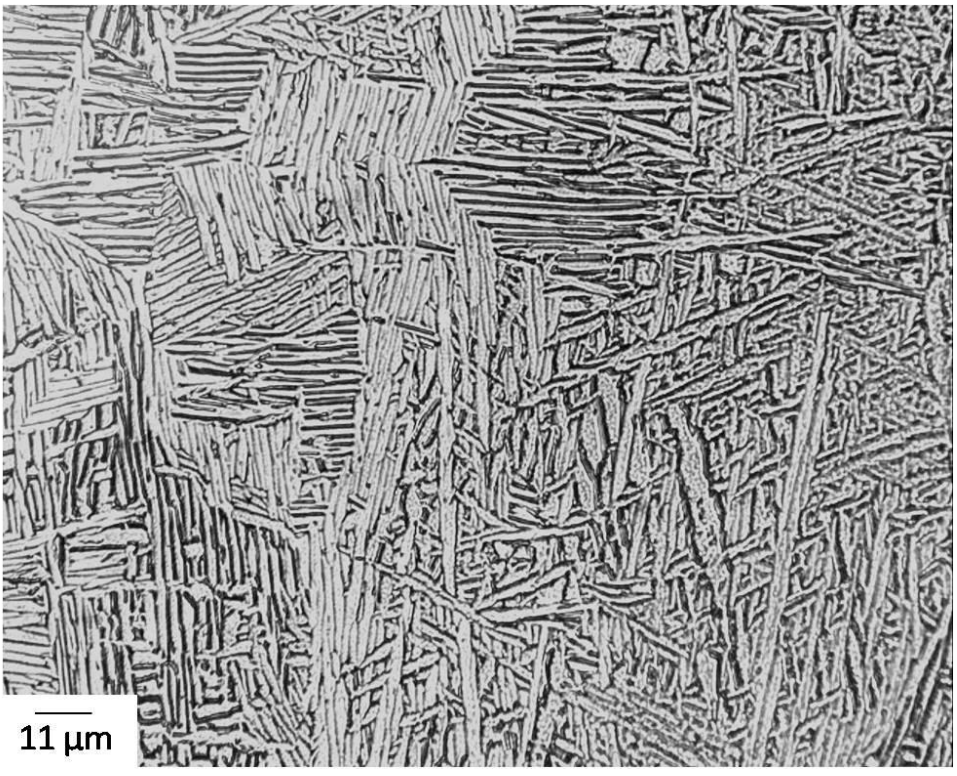

Figure 4.5.2 EBM component: Focus 30, 400mm/s and 6mA

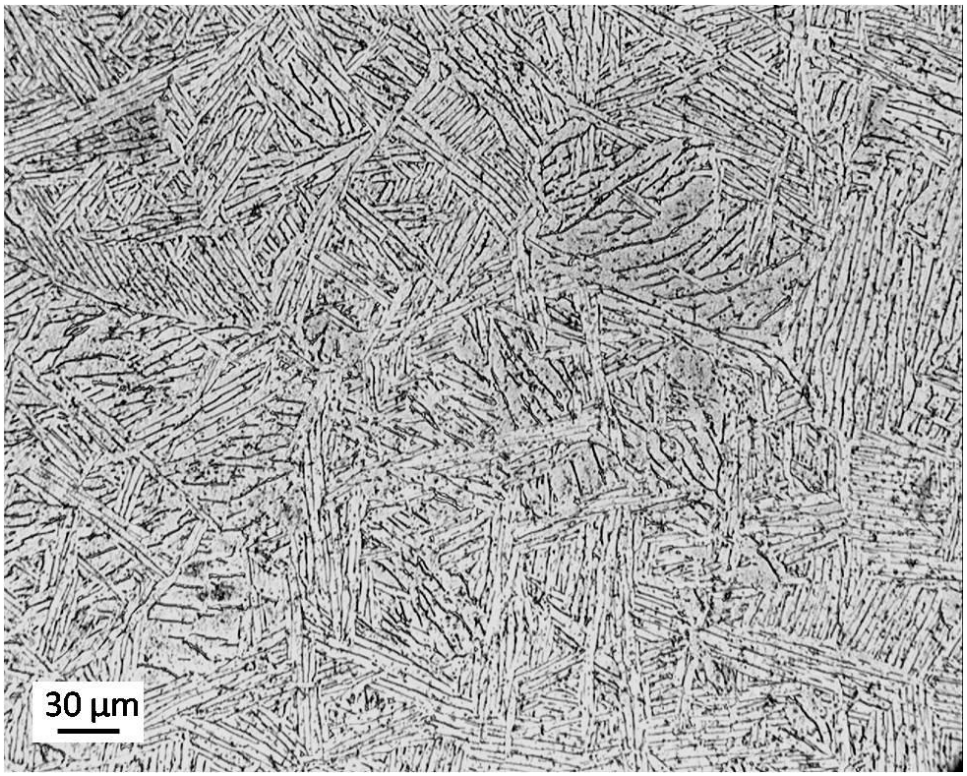

Figure 4.5.3 EBM component: Focus 30, 400mm/s and 6mA, top section of 2 passes

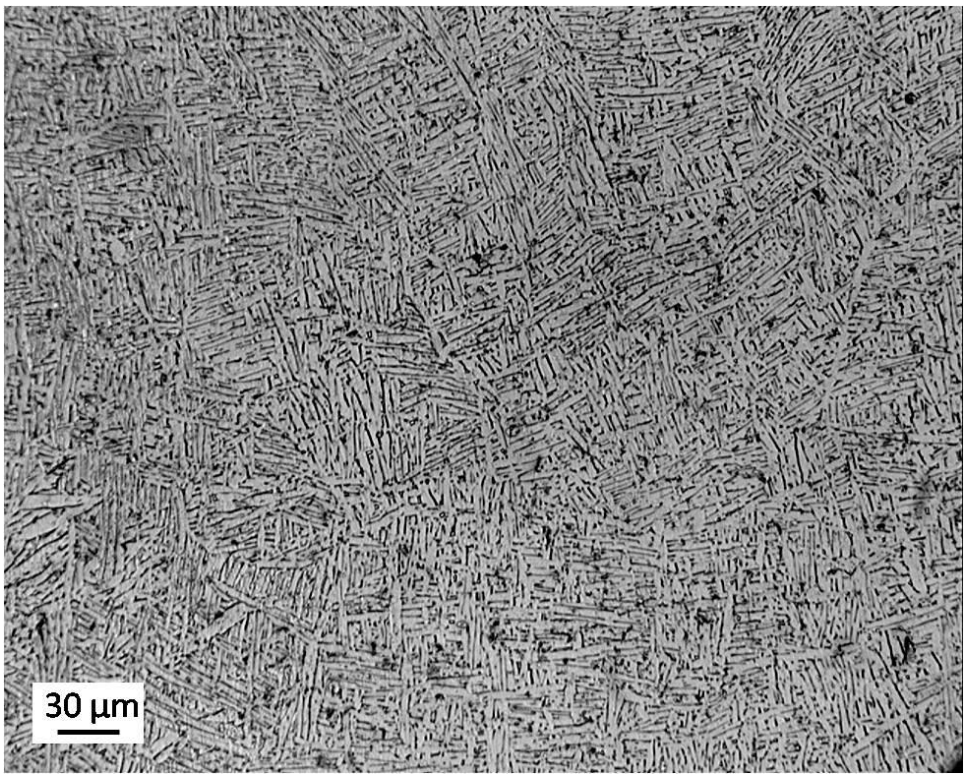

Figure 4.5.4 EBM component: Focus 30, 400mm/s and 6mA, bottom section of 2 passes

After performing microstructural analysis on solid components, Ti-6Al-4V mesh builds were also cut, ground, polished and etched for microstructural analysis as well. The obtained microstructure exhibited predominantly α'-martensite as shown in figure 4.5.5. The corresponding microstructure of mesh components also exhibited higher hardness values than solid components. By comparing a solid component of 2 cm in thickness with a mesh component roughly 0.3 cm thick, it can be assumed that the cooling rate of the mesh components is higher and therefore a martensitic structure is provided with the corresponding higher hardness values. Figures 4.5.6 and 4.5.7 show microstructural differences in size due to the number of times the melting beam passed through the powder, showing two and three passes, respectively.

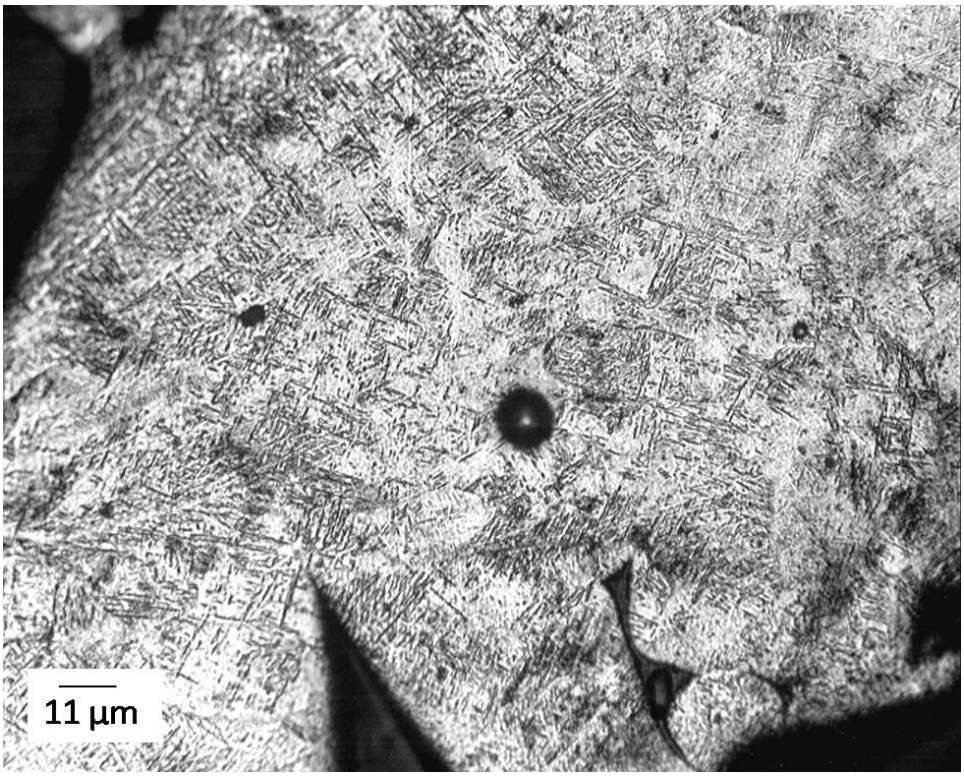

Figure 4.5.5 EBM mesh component

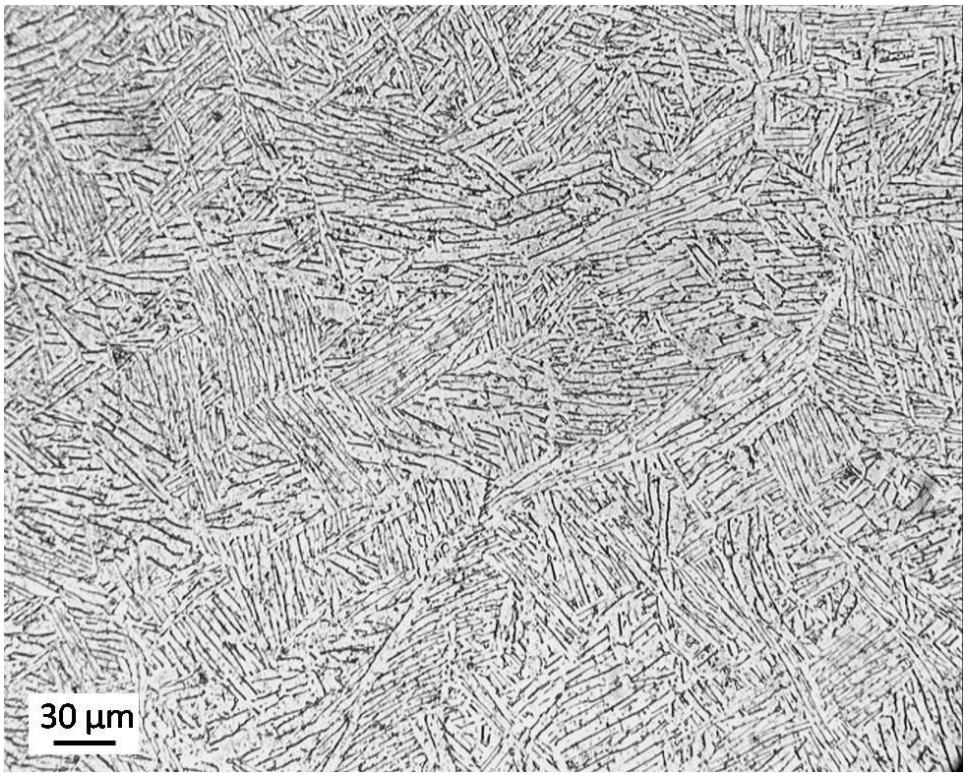

Figure 4.5.6 EBM cylinder component: top section of 2 passes

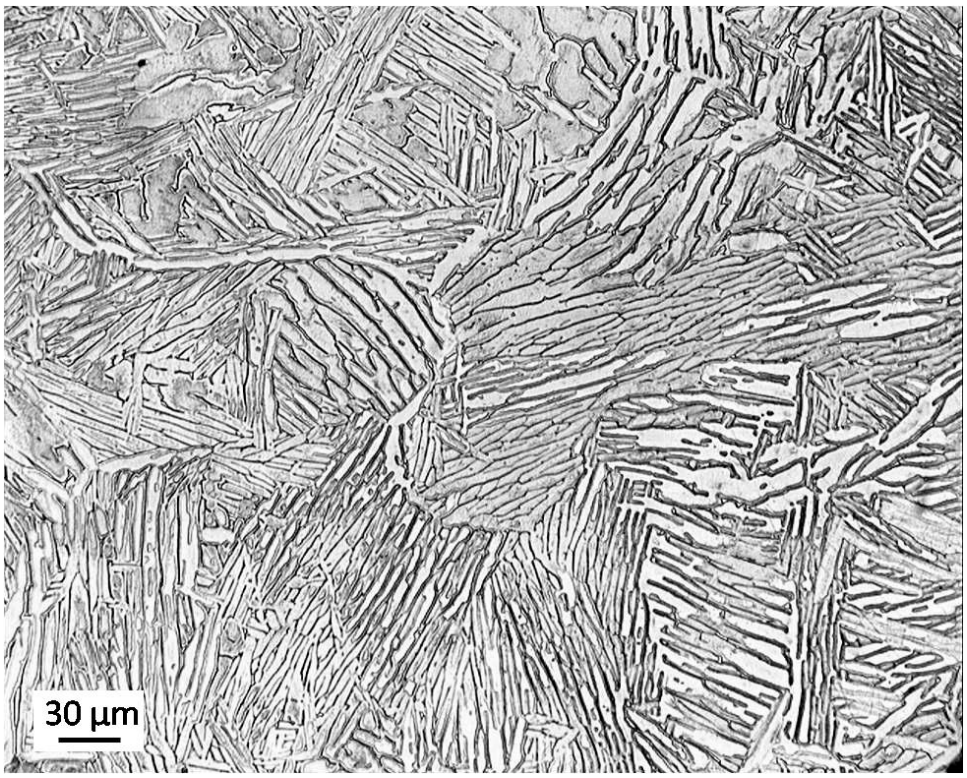

Figure 4.5.6 EBM cylinder component: top section of 3 passes

Ti-6Al-4V foams, shown in figure 4.3.5 and obtained out of an aluminum foam CT scan, were metallographically analyzed to obtain a mixture of α and α'-martensitic microstructure, see figure 4.5.7. It can be stated that hcp α is transforming into α'-martensitic as the sample gets thinner and lighter. Additionally, as the number of melt scan passes increases, the microstructure grows as can be observed in figure 4.5.8. Figure 4.5.8 shows the microstructure of three different standard cylinders with the same parameters but different number of times that the melt scan passed through the powder layer, the magnification is the same for the three samples.

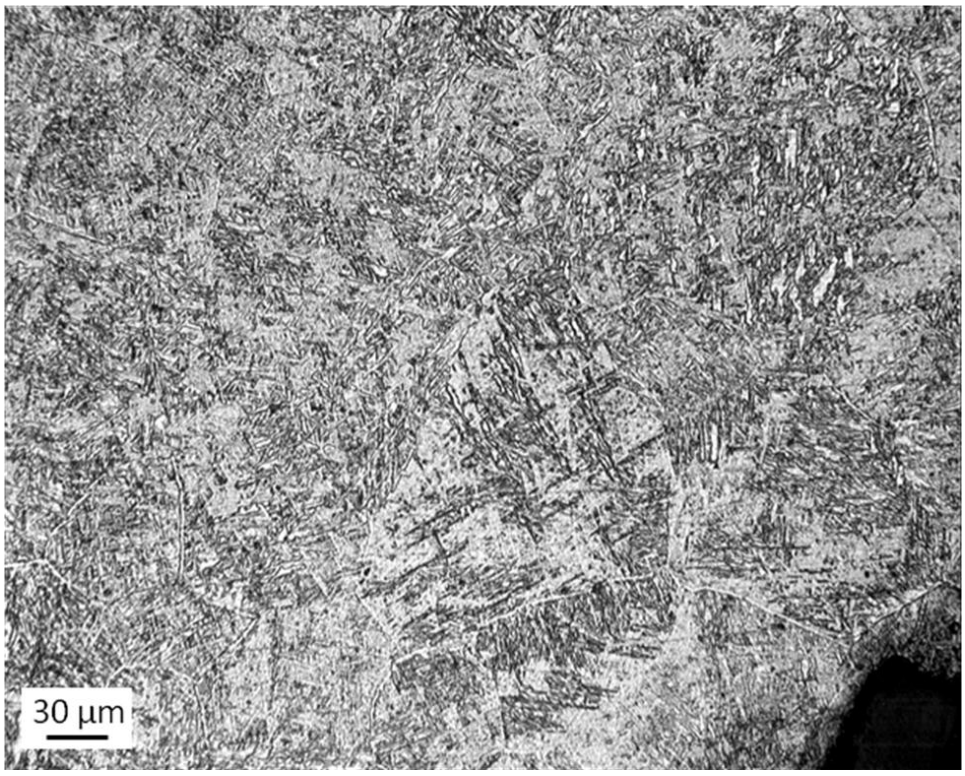

Figure 4.5.7 Ti-6Al-4V foam

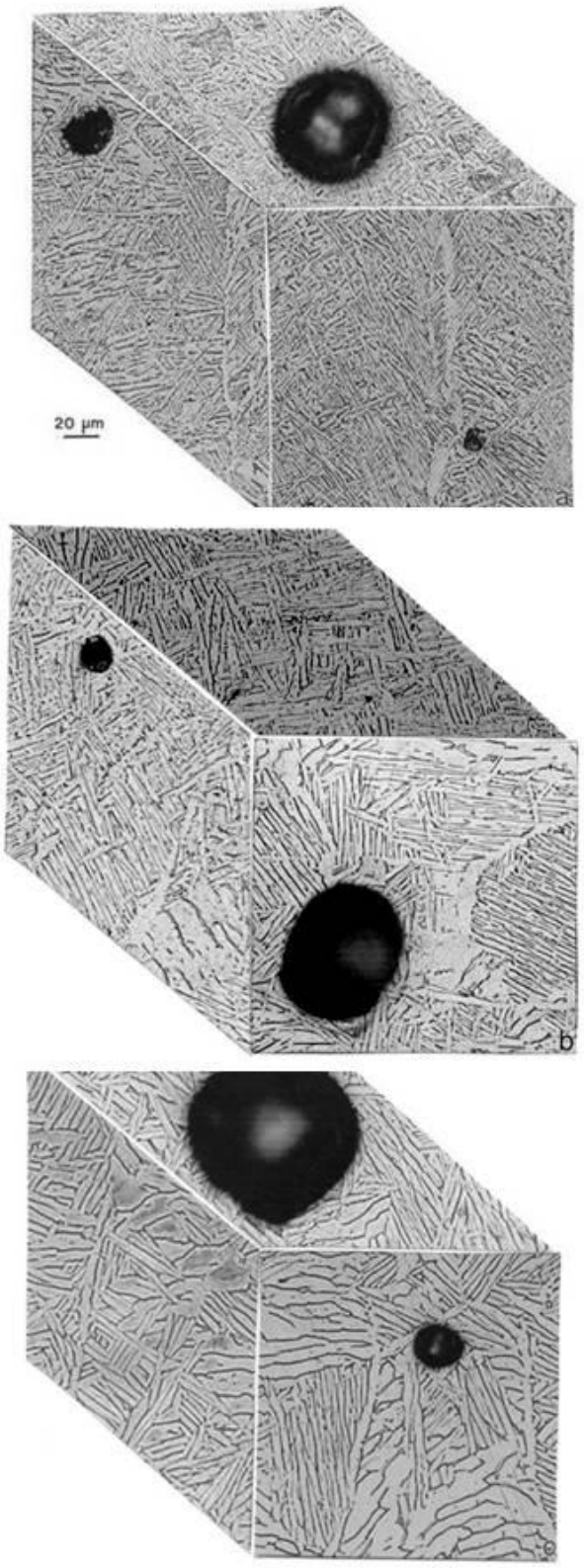

Figure 4.5.8 Ti-6Al-4V cylinders. a) one melt scan, b) two melt scans, c) three melt scans

4.6 Mechanical Properties

Hardness testing was performed on solid components of parameters of 400 mm/s for the melt scan speed and a lens current of 6 mA with a focus of 26 and 30. These components showed HRC hardness values ranging from 35 to 38. Tensile testing was performed on standard cylinders at a focus of 30 (lens focus setting) that required the use of special grips to place the specimens in the Instron machine. An elongation variation from ~12 to 25% was obtained and an ultimate tensile strength (UTS) of 1.1 to 1.4 GPa was observed. Tensile test analysis was also performed on standard cylinders having the same parameters but instead of a single pass in the melt scan, the specimen had three passes. UTS obtained for the three passes in the melt scan varied from ~1.2 to 1.3 GPa.

As already mentioned, tensile testing was performed at room temperature and fractured surfaces were analyzed under the scanning electron microscope the day after the test. Figure 4.6.1 shows SEM micrographs depicting the fractured surface for the specimen at a focus of 30, already mentioned. The microscale presence of dimples on the fractured surface is a characteristic indication of ductile fracture [24]. It can be observed in figure 4.6.1 and 4.6.2 the presence of dimples in the fractured surface of the tensile specimens. Figure 4.6.2 represents the fracture surface of a sample with three melt scan passes.

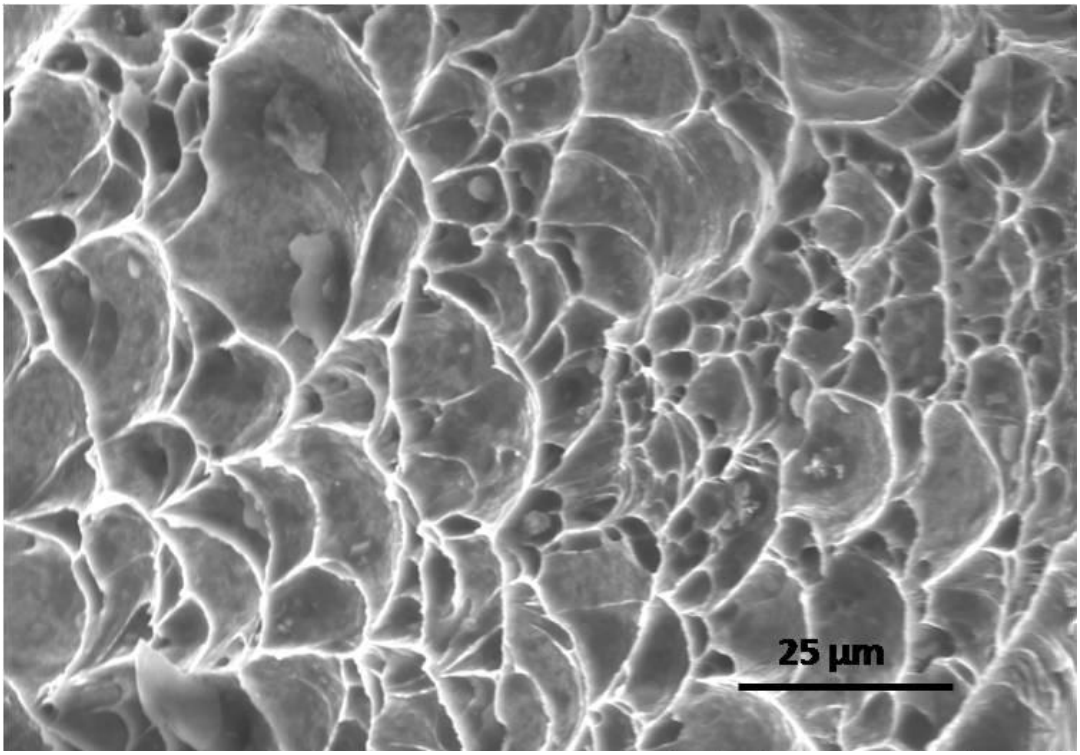

Figure 4.6.1 Tensile fracture surface of specimen with a focus of 30

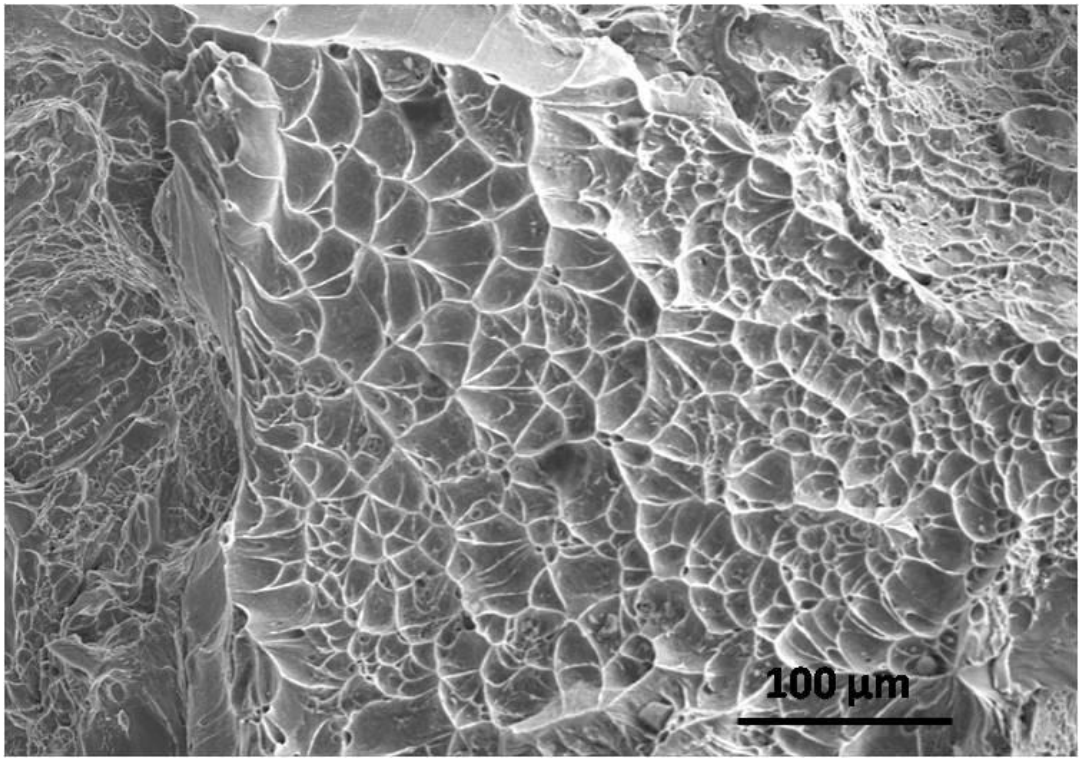

Figure 4.6.2 Tensile fracture surface of specimen with triple melt scan passes

Rockwell Hardness C-scale testing was also performed on solid components of 2 and 3 melt scan passes, ranging from 35 to 37 HRC, having the highest values for the specimen with only 2 melt scan passes. Figure 4.5.3 shows the top section of a double melt scan with a corresponding HRC average value of 36 while the bottom section shown in figure 4.5.4 has an average HRC value of 37. Even when the difference is only by one unit it can be observed that microstructural features relate to hardness values: having the more compacted microstructure at the bottom the higher hardness values.

For the mesh components shown in figure 4.3.7 Vickers hardness (HV) testing was performed obtaining values ranging from 367 to 411, which translated to HRC values ranging from ~37 to 42. It can be observed how mesh components had a little increase in hardness compared to solid components. Due to the porosity in mesh and foam components, tensile testing was omitted. The Vickers hardness for the foam component was ranged from 411 to 466 which in HRC is from 42 to 46. Again, as the thickness of the components was decreased, finer microstructure was obtained and therefore, hardness values were increased.

4.7 Transmission Electron Microscopy

The first time sample preparation for TEM was performed was on 1x1x1 cm^3 with no parameters set. Interestingly enough, a lot of uncommon situations occurred on the samples; images were not clear enough to see, it was like some additional film was on top of the 3mm disk that would not let to obtain a clear focus on the microscope, even when shiny specimens were obtained from the electro-polish. The next set of samples prepared

for TEM consisted of thin sections of the standard cylinders with a focus of 30, current lens of 6mA and 400mm/s as scan speed. Two different types of samples were prepared with the same jet-polishing parameters as before, 13V and a -15°C temperature in a solution consisting of 900mL of methanol and 50mL of sulfuric acid. The difference on these two types of samples was the number of melt scan passes. On one side, a set of samples consisted of a single melt scan pass while on the other side; three passes were used for the melt scan. Figures 4.7.1 to 4.7.3 show transmission electron microscopy images with their corresponding diffraction pattern for a single melt scan while figures 4.7.4 to 4.7.5 correspond to a triple melt scan.

Figure 4.7.1 shows the corresponding microstructure observed in the optical microscope, α-grains surrounded by the β-phase with a dislocation density of $\sim 10^7/cm^2$ with its corresponding diffraction pattern [25]. Figure 4.7.2 shows a higher magnification in the α-grain where a dislocation network can be appreciated. As stated by Sugui, in nickel base super alloys the dislocation networks are formed to relieve coherency stress enhancing the creep resistance [26]. Therefore, by having dislocation networks in Ti-6Al-4V alloy we may expect properties being enhanced. The corresponding diffraction pattern is shown. Figure 4.7.3 shows a single pass melt scan image with the lowest magnification showing the corresponding α grains with β surrounding as well as the presence of dislocation defects and the corresponding diffraction pattern. It can be appreciated how in one of the α grains a dislocation network started to form.

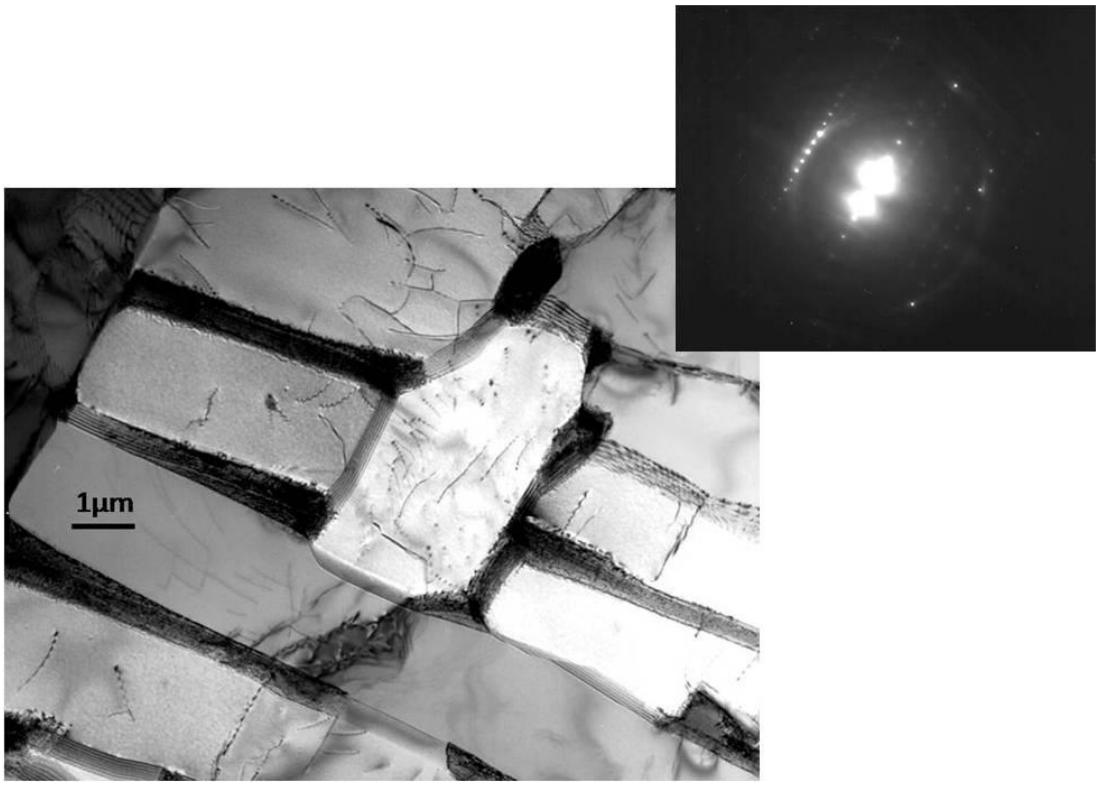

Figure 4.7.1 1 melt scan: α grains surrounded by β boundaries

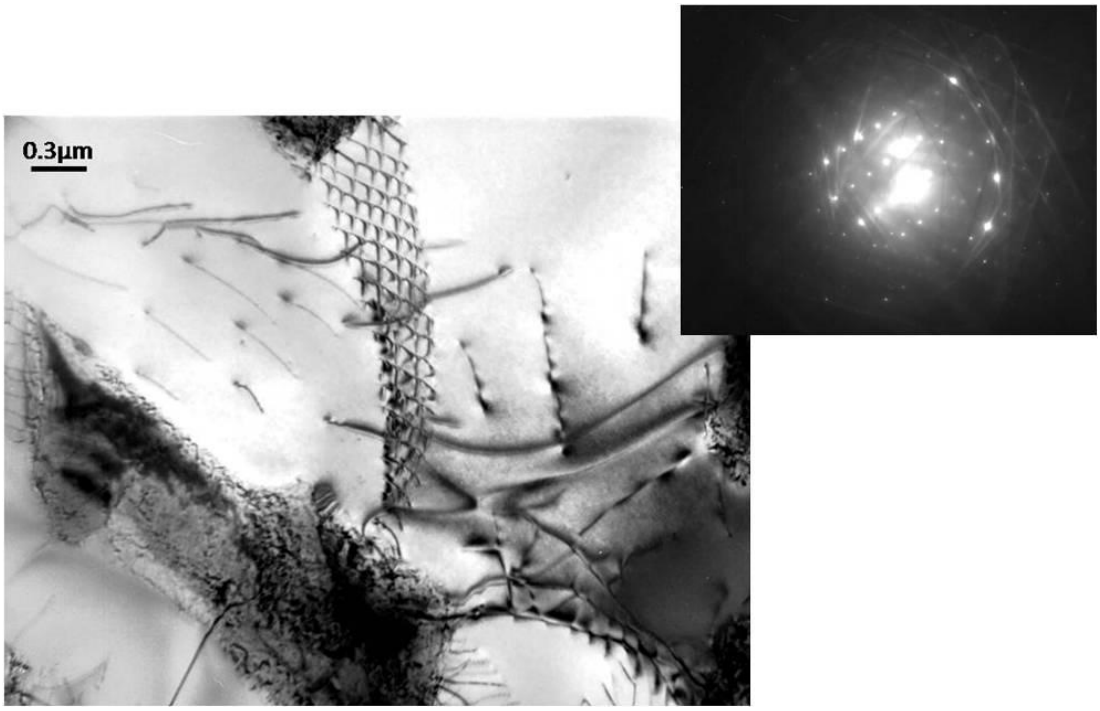

Figure 4.7.2 1 melt scan: higher magnification showing a dislocation net

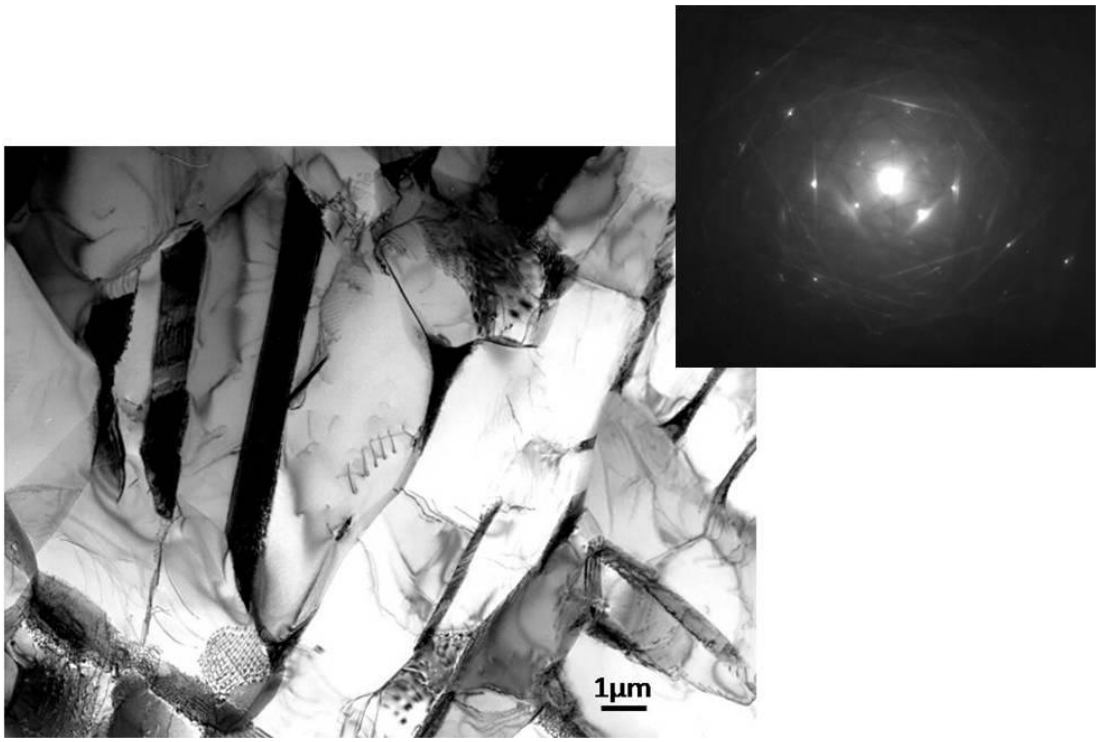

Figure 4.7.3 1 melt scan: α grains showing dislocation defects

Triple melt scan images are shown from figure 4.7.4 to 4.7.6 as already mentioned. All triple melt scan pass images are at a higher magnification than the ones already shown for a single melt scan pass. Basically, the three micrographs show different α-phase grains with dislocation defects inside. It can be appreciated how the corresponding diffraction patterns for triple melt scan passes show a similar curvature with more than one main diffracted beam, probably representing the dislocation defects diffracting the most. Figure 4.7.6 shows a set of dislocation steps showing dislocation cross-slip. When there are two or more slip planes with a common slip direction, cross-slip can occur in slip planes [27].

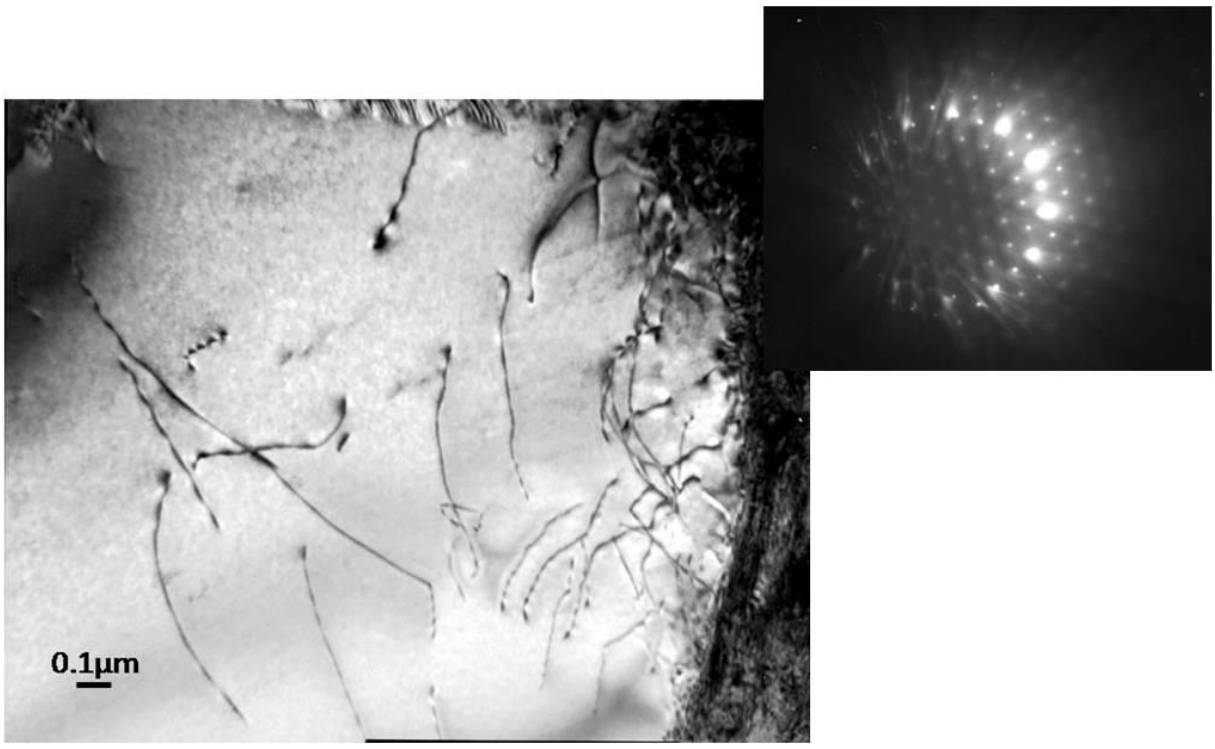

Figure 4.7.4 3 melt scan passes: high magnification image of dislocation defects

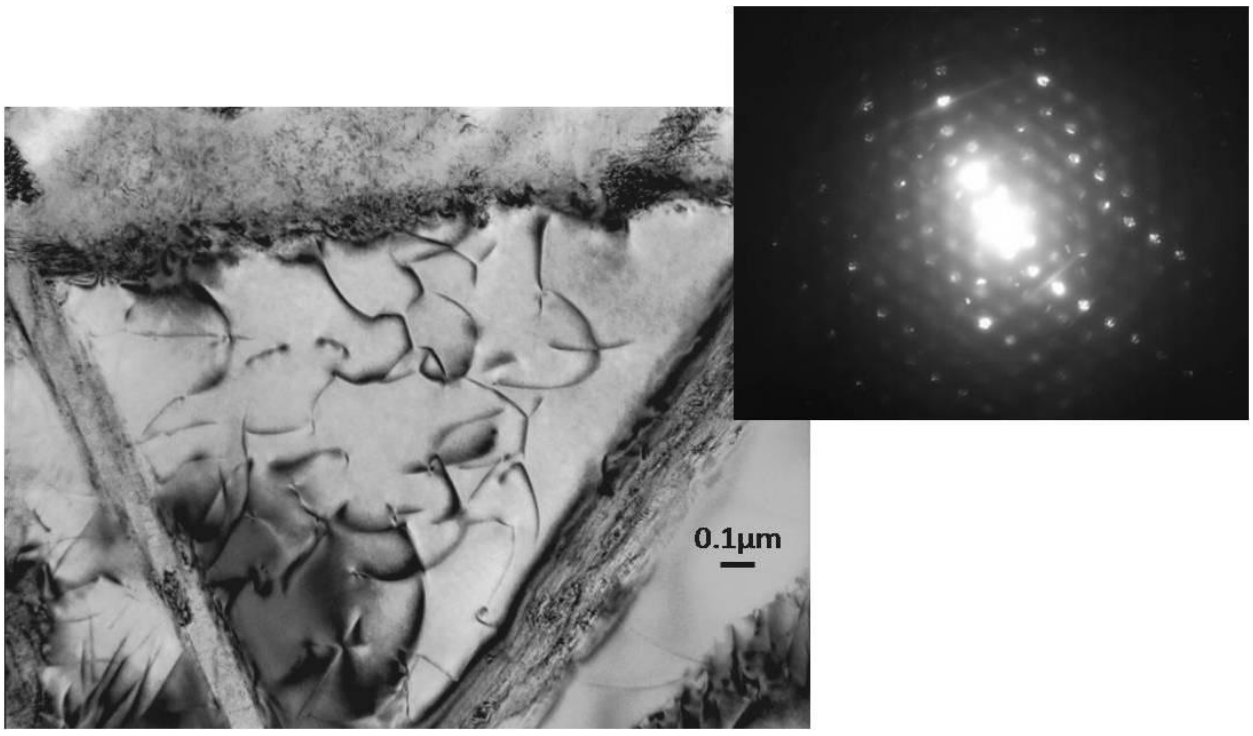

Figure 4.7.5 3 melt scan passes: dislocation defects in α-phase

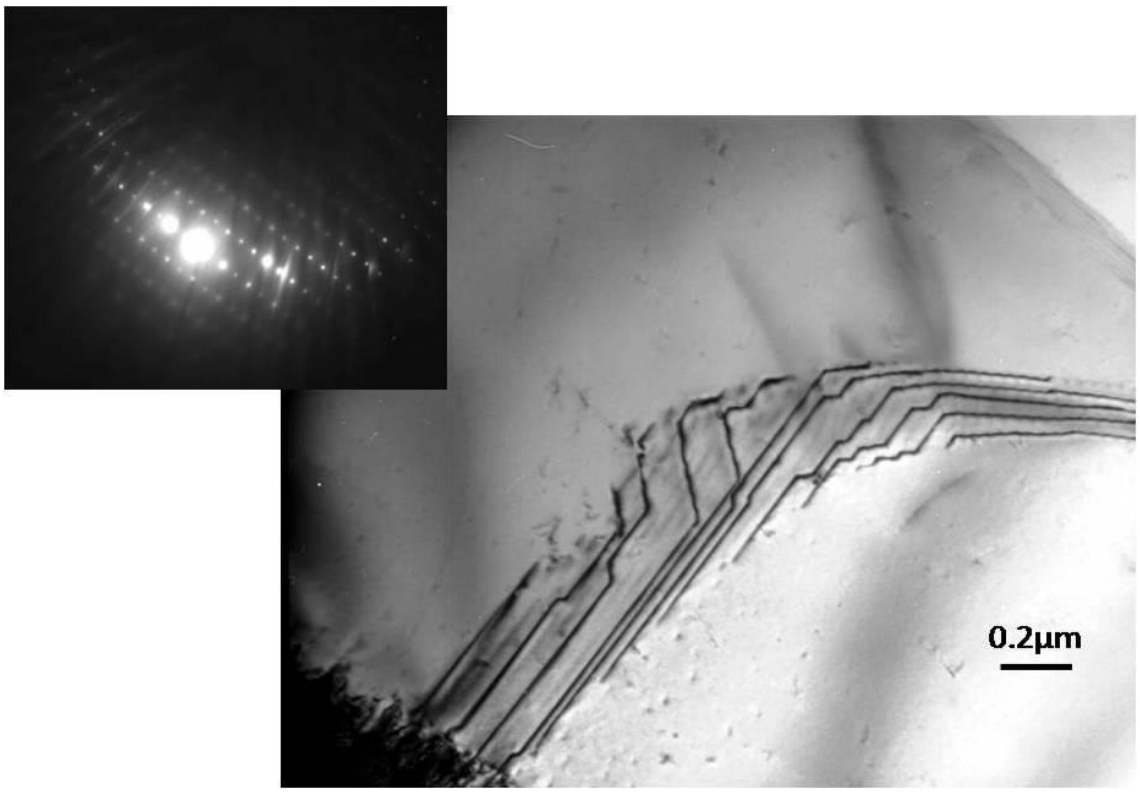

Figure 4.7.6 3 melt scan passes showing dislocation steps

In order to obtain transmission electron microscope images out of mesh and foam components, a different build had to be designed. Since mesh and foam components are too thin in any direction as to create and/or prepare thin specimens for the TEM, a specific geometry was designed that simulated the thickness of the mesh and foam components. Besides simulating the thickness of the specimens, what is more important is that the cooling rate for thin specimens was desired to be the same for the designed component.

Figure 4.7.7a shows the CAD designed as sent to the ARCAM EBM A2 system while letter A in the image shows how thickness was varied throughout the specimen. Figure 4.7.7b shows the actual EBM built fabricated. It can be appreciated how small squares of approximately $1cm^2$ have a thickness of ~1mm. Once the desired areas were cut, the

specimen was glued to a flat polymer mount and carefully ground to obtain the desired thickness, punched and electro-polished with the same jet-polished parameters used for solid components.

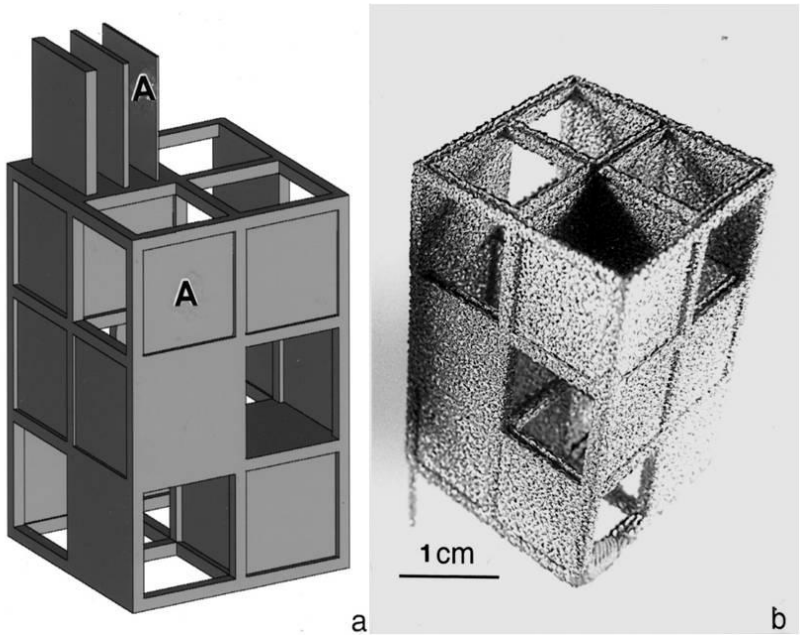

Figure 4.7.7 a) CAD design of component simulating thin specimens. b) fabricated component

Figure 4.7.8 and 4.7.9 show TEM images obtained from specimens obtained from the top portion of the build shown in figure 4.7.7. By comparing figure 4.7.1 and 4.7.3 with figure 4.7.8 it can be appreciated how the last one has a finer microstructure, since the three micrographs are at relatively the same magnification. From optical micrographs, it can be stated that figures 4.7.8 and 4.7.9 represent the presence of α'-martensitic phase structure, as well as dislocation defects inside the grains. It can also be observed how both micrographs show a more complex diffraction pattern, resulting from both α and β diffracting phase regions.

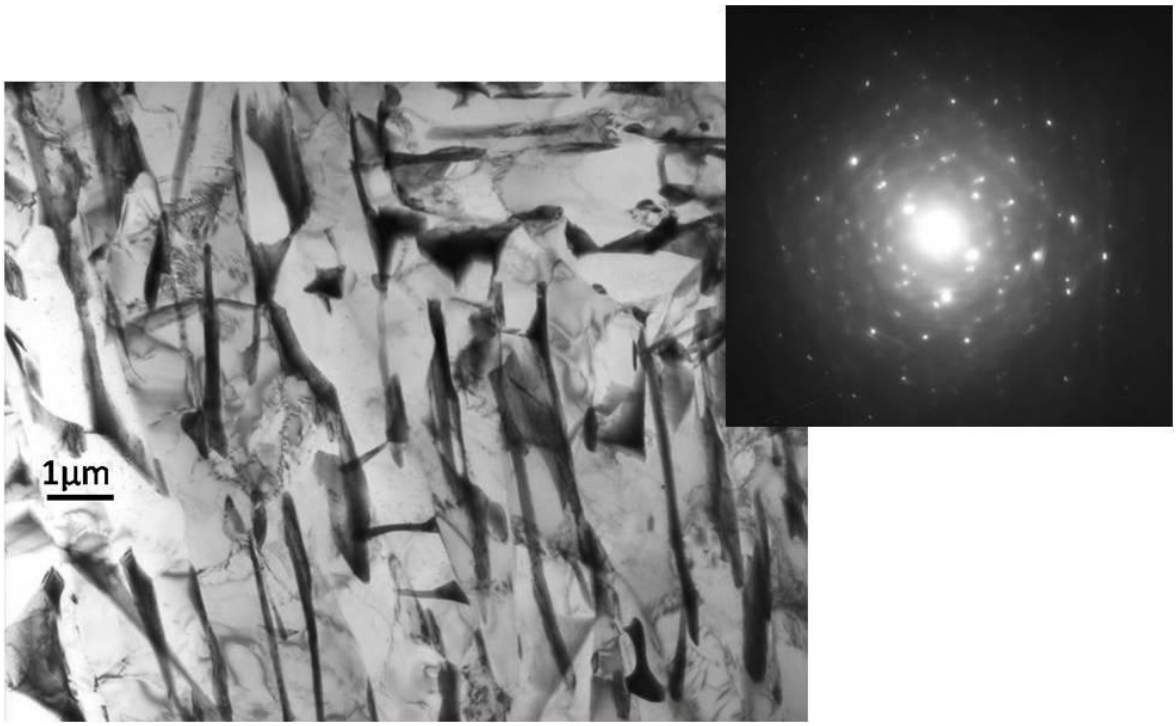

Figure 4.7.8 Specimen simulating mesh and foam components

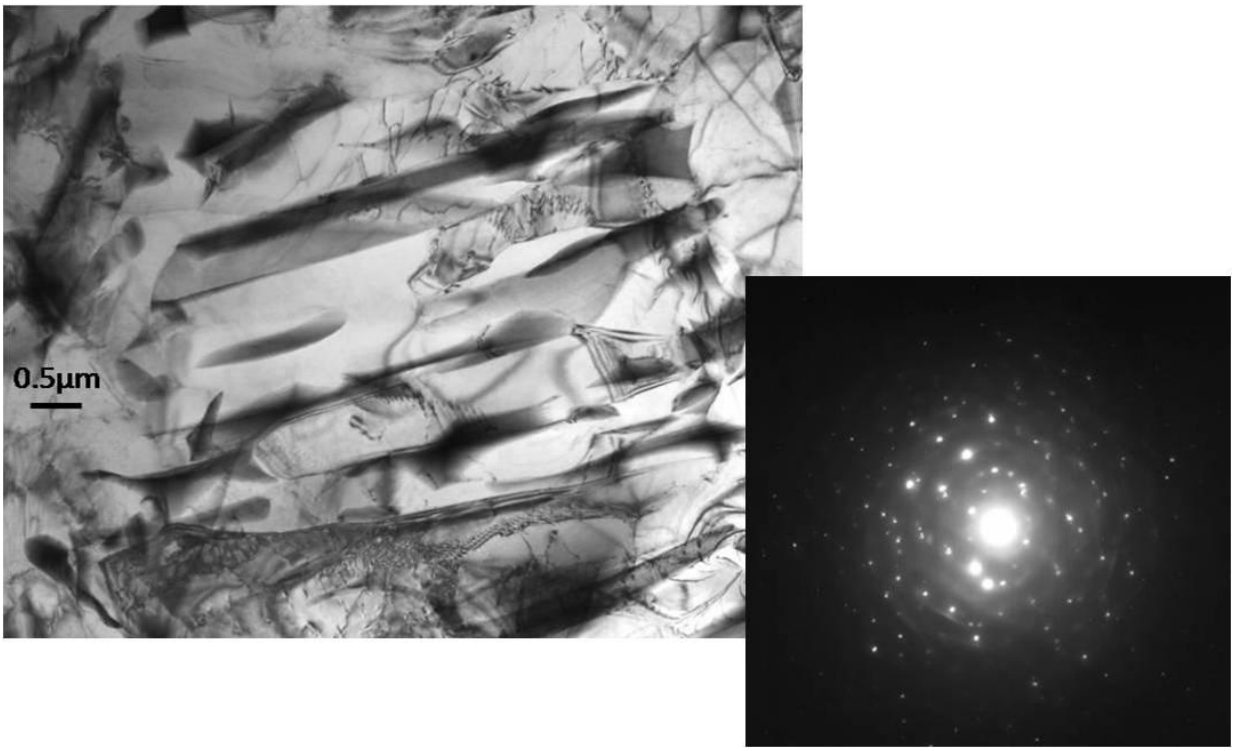

Figure 4.7.9 TEM micrograph of component shown in figure 4.7.7

Besides analyzing TEM specimens in the H-8000 microscope, samples simulating mesh and foam components were place in the H-9500 microscope. Figure 4.7.10 shows an image obtained from the HRTEM showing the same structure observed in figures 4.7.8 and 4.7.9, representing the α' structure observed in the optical microscope. Dislocation defects can also be observed from the image. It must be stated that certain error belongs to the marker since the instrument is not calibrated accurately. The only reason why this micrograph is shown is to provide an image of higher magnification for the samples simulating mesh and foam cooling rate components.

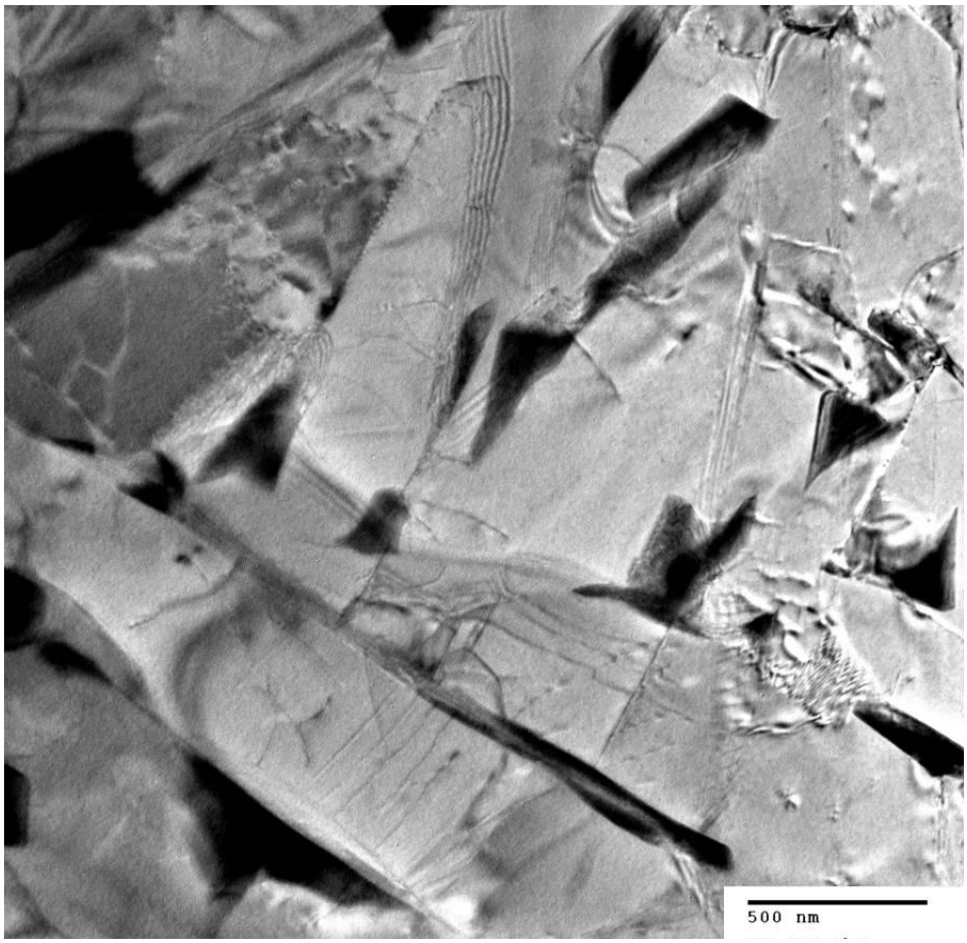

Figure 4.7.10 HRTEM micrograph of component shown in figure 4.7.7

4.8 Quality Analysis and Control

Widely speaking, electron beam melting manufacturing implies a two step process, designing and component fabrication. At the time of selecting the system parameters variation in microstructure will occur. Quality control or quality assurance (QC or QA) can be descriptive of the process by comparison without component's destruction. Monitoring each layer by the creation of build logs with temperature profiles, beam irregularities, including preheat and melt cycles, occurs in additive layered manufacturing by EBM. By performing a QC analysis the first aspect to consider would be the build log trying to detect any irregularities that could be related to build flaws or defects, such as unconsolidated regions. This can be achieved by building prototypes of a certain form of witness coupons or QC tabs to be easily detached for analysis purposes from the main component. The main component is then dissected and compared to their corresponding QA tabs.

A specific component was fabricated in the ARCAM EBM system with 11 detachable tabs located in different locations of the build. Various tabs were randomly selected and microstructurally compared with the corresponding section in the build. Figure 4.8.1 shows the build component and a microstructure comparison, it can be appreciated how detachable tabs located in the back required support material at the time of being fabricated. Once the tab was detached and the component dissected, optical metallography was performed on the specimens. It can be appreciated how, being at the same height, both micrographs show an acicular α-microstructure of similar size, both micrographs were taken at the same magnification. A proper process optimization could be improved to obtain a better correlation with the build log and the further analysis.

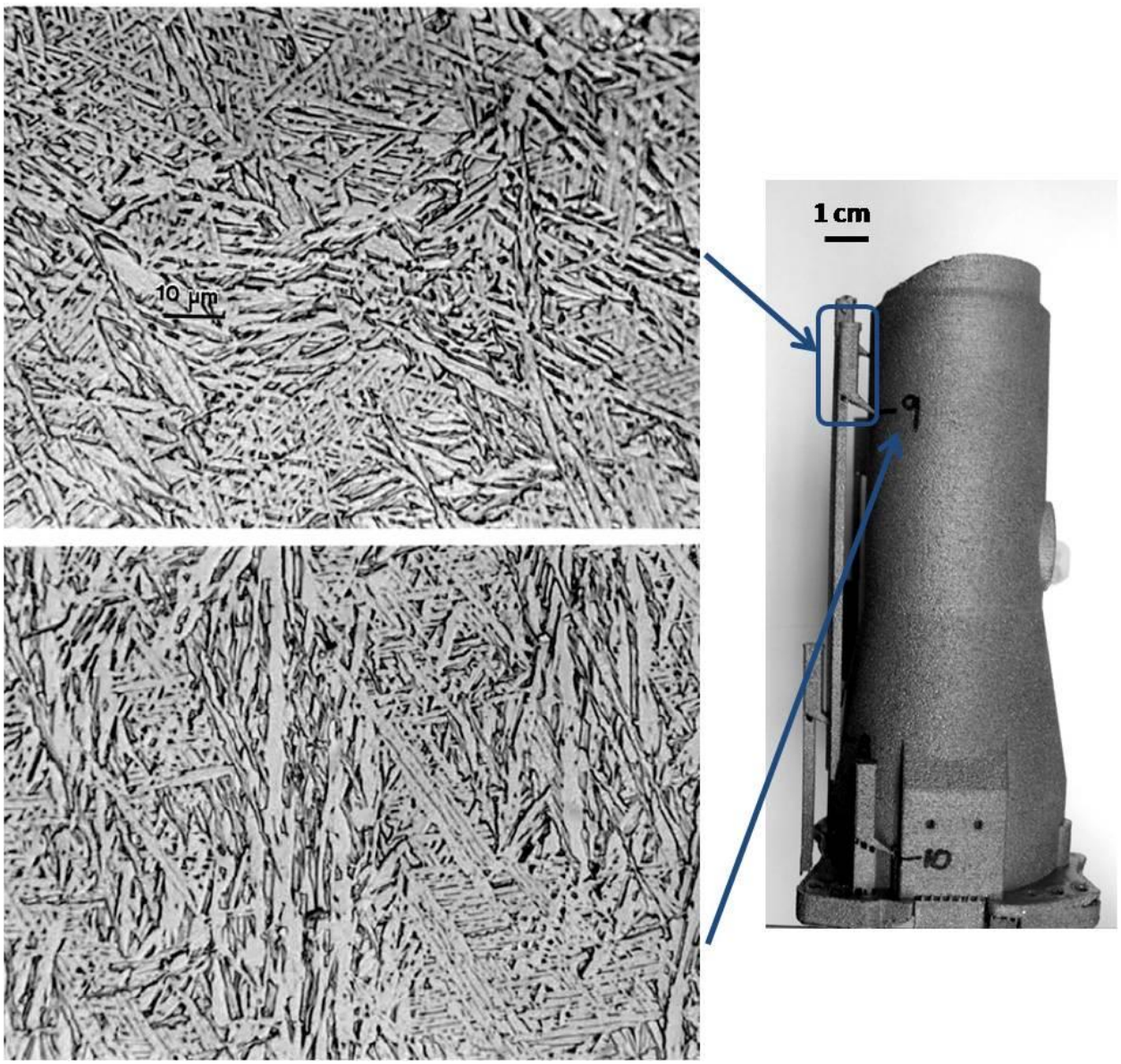

Figure 4.8.1 Microstructure comparison of detachable tab and build component

4.9 Ideal applications

It is important to mention that this section implies what an ideal application could be for EBM fabricated components. The most incredible aspect of this technology is the fact that anything can be customized to individual needs. What is meant by this is that a CAD design can be created of what is needed and fabricated by less expensive technologies, such as Z Corp 3D Printing, inspected by the costumer to check everything is as required and then continue the process by fabricating the component by additive manufacturing using EBM technologies with Ti-6Al-4V powder.

One main area that could benefit from the properties obtained out of EBM components is the biomedical field. Hip and knee implants can be easily fabricated to specific dimensions. Generally, Ti-6Al-4V is used for joint replacement components because of its superior mechanical properties. Besides, one of the main factors considered by orthopedics is the importance of the implant form, such as macrotexture desired for the stability fixation in bone. Moreover, research studies results show that by increasing the implant roughness the bone response can be enhanced [12]. Moreover, fixation by bone ingrowth rather than cemented prosthesis has given good clinical results by the use of porous coatings in surgical implants [28]. Ti-6Al-4V has been considered a good selection for implant applications due to the alloy's strength to weight ratio, in addition to its outstanding corrosion resistance, biocompatibility and lower modulus of elasticity [13]. One advantage of fabricating hip stems utilizing EBM technology is that the porous surface, that will allow bone ingrowth, can be built on the same step of the fabrication process [29].

Nevertheless, implant components need the appropriate ASTM standards to be recognized or more specifically to be set. Proper analysis need to be performed such as

chemical composition, microstructural and tensile aspects as well as fatigue, and more importantly, it is necessary to know how bone and surrounding tissue will respond to the EBM fabricated component. Of course, a lot of research and testing needs to be done before this can become our new reality.

Figure 4.9.1 shows fabricated EBM cylinders as well as CAD designs, figure a) shows the actual fabricated cylinder with an outer density higher than the inner density, while figure b to d) show CAD designs with different inside structure. Figure 4.9.1 b) shows an outside specific structure while the inside corresponds to a foam component. It can be appreciated in figure 4.9.1c) that both the outside and the inside have a certain geometry that will provide different porosities and therefore different densities. Figure 4.9.1d) shows the top view of figure 4.9.1b).

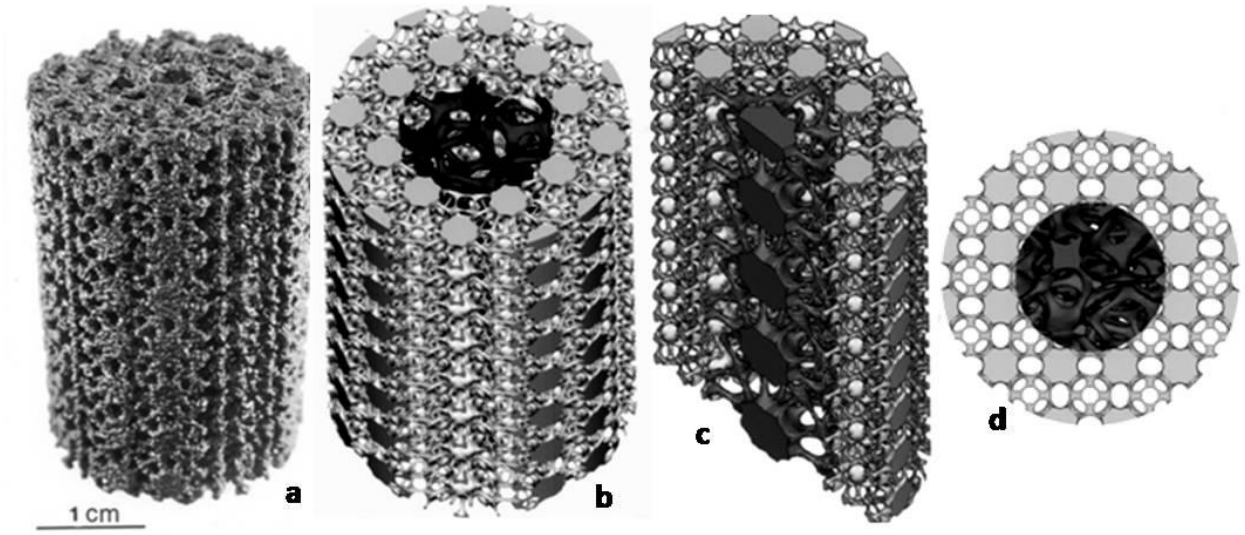

Figure 4.9.1 Fabricated and CAD designs of cylindrical components

Figure 4.9.2 shows the CAD design of the fabricated Ti-6Al-4V EBM component shown in figure 4.9.1a) and how these rods could be inserted in fractured bones as depicted by the arrows. From the bone image it can be observed how the outside structure is more compacted than the inside structure, therefore, the same is simulated by the cylindrical component. The same type of situation is simulated in figure 4.9.3 with the aid of a fake bone made out of solid foam.

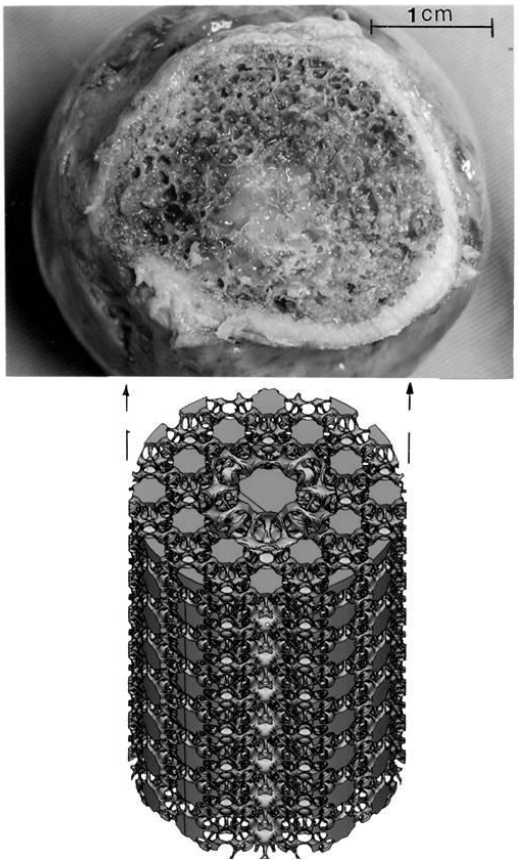

Figure 4.9.2 CAD design of cylindrical components that could be inserted in fractured bones

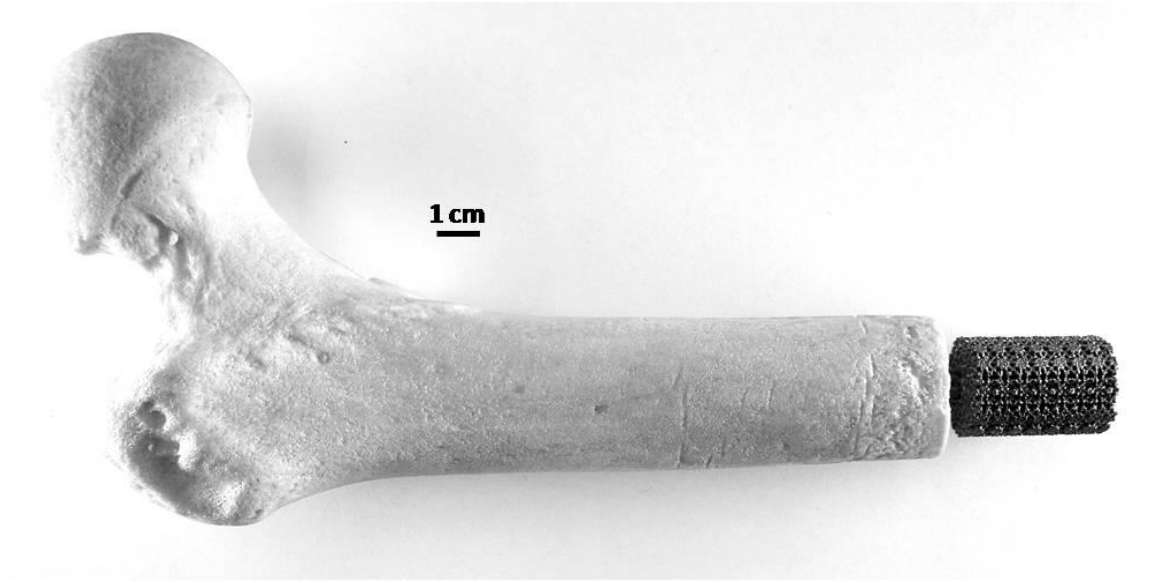

Figure 4.9.3 Simulation of ideal use for EBM components with desired porosity

Bone consists of two main aspects, outer cortical bone: which is a dense structure with high mechanical strength, and the inner trabecular bone: which consists of large voids, with 55-70% interconnected porosity [30]. As mentioned before, different porosities and structures can be obtained out of the ARCAM A2 system. It is implied that solid, mesh and foam components can be fabricated with different densities according to specific needs. Figure 4.9.4 can be an ideal example where the cortical bone stiffness and density are simulated by EBM components where the outside foam structure has a lower density than the inside, which is characteristic of trabecular bone. Of course, different research studies have to be performed to find out how bone tissue will react before any of this can be implanted.

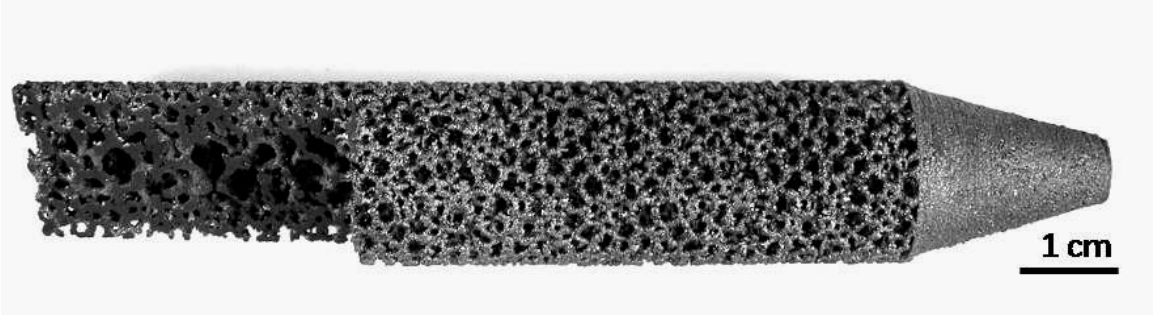

Figure 4.9.4 Foam component cut to show half section view

Besides the biomedical applications for Ti-6Al-4V, the aerospace field could be benefited as well. Providing the benefit of creating desired complex geometries, the aerospace industry could take advantage of this. According to Javidrad, original aerospace components are ignored and re-designed completely in accordance to the performance requirements and interfacing constraints (space/weight for example) [31]. More sophisticated avionic systems for civil and military aerospace industry is under constant pressure to create them at lower cost [32]. Other research projects have been analyzing electron beam welded test pieces, of Ti-6Al-4V for potential aerospace component cleaning application, by laser irradiation before joining, producing acceptable joint strengths and microstructures [33]. It is understood that only small, and precise, components can be fabricated by electron beam melting in the ARCAM A2 system to fullfill aerospace applications and become a possible way of manufacturing components.

One more example of how additive manufacturing using EBM fabrication could be applied is in the artistic field. Ballet toe shoes are handmade fabricated in a layer by layer fashion by using different types of cardboards and glued together, this conical toe box consists of layers of burlap, cardboard, or paper, or a combination of them. These layers rigidify the toe box when the adhesive cures [34]. Figure 4.9.5 shows a pointe ballet shoe

showing the addition of layers used to construct the toe box shown by the square. The downside of these ballet shoes is the fact that the lifetime depends on the usage since sweat deteriorates the shoe in a fast basis. As of today, specific pointe shoe brands provide a vertical strength of ~520N (117lbf) on static load [35]. EBM technologies can improve this by creating a Ti-6Al-4V outline box that will increase the lifetime of the shoe. However, plenty of cushioning material, such as soft plastics, must be used on the inside of the box to prevent bruises and injuries in the dancer, as well as a layer of plastic on the outside to minimize noise at the time of impact.

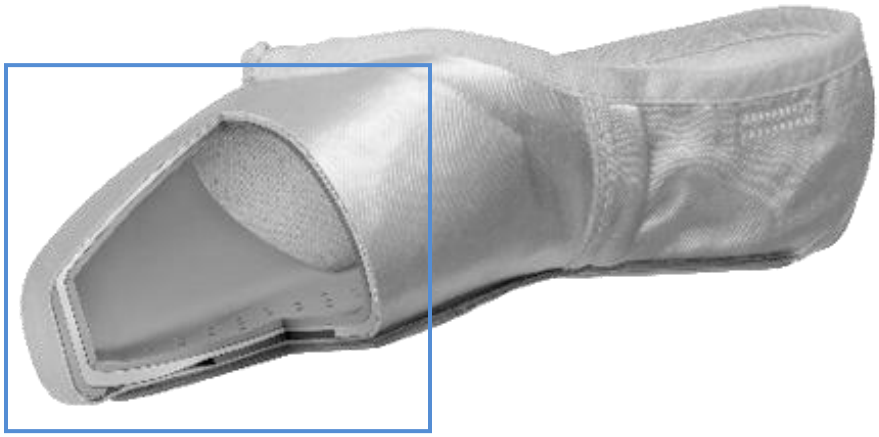

Figure 4.9.5 Pointe shoe showing toe box representing layers glued together

These are only some examples given of how EBM manufacturing can be used to improve specific fields. But still it is important to mention that any component fabricated that will be responsible of somebody's body needs to go through a lot of research and testing before it can become commercially available.

CHAPTER 5

SUMMARY AND CONCLUSIONS

Ti-6Al-4V is an alloy widely utilized in different fields such as biomedical, automotive and aero spatial, among others [8](Gerd Lutjering, 2003) One of the reasons why this alloy is better for certain applications is due to its high fatigue strength as well as tolerable temperature capability, in addition to the excellent balance in mechanical properties, high strength to weight ratio and the excellent corrosion resistance and human allergic response and excellent biocompatibility [36].

It has been demonstrated how Ti-6Al-4V can be created on a CAD design and fabricated in a layer by layer fashion by melting and consolidating powder particles with the aid of EBM system, more precisely, the ARCAM A2 machine. After proper optimization of the system's parameters, several components were fabricated and analyzed. When it was realized that different geometries, and densities, could be achieved from this technology, they were fabricated and analyzed as well. In summary, the three different types of components produced and examined consist of fully dense solid components, geometrical mesh components and foam components of different densities.

The first concern regarding the use of EBM systems is whether the aluminum content in Ti-6Al-4V might be reduced during the manufacturing process. After analyzing powders utilized at different stages of the fabrication process, results show that both aluminum and vanadium weight percent remained fairly precise in a range of 6.47 to 7.11% and 3.2 to 4.6% respectively. It can be appreciated how the element being reduced in the process turned out to be the vanadium, by only a 0.8% reduction, providing enough

information that allow the powder recycling. Furthermore, an analysis of recycled powder particles was conducted and it was found that even when the particles size range is from 3 to 100μm with an average particle size of 46μm, a bimodal distribution can be appreciated with an average of 17μm for the small size particles and 59μm for the bigger size particles.

The analysis of the fabricated specimens consisted in an irregular-shape porosity diminution in solid components achieved by the optimization of the ARCAM EBM A2 system; results show that the best parameters to be utilized consist of a scanning melt scan speed of 400mm/s and a lens current of 6mA with a focus of 30. After parameters optimization some spherical-shape voids remained in the components and with the analysis of start and prep powder it was found that these spherical voids are obtained from the gas atomization process responsible of creating the Ti-6Al-4V powder, since gas is trapped in certain particles and retained throughout the process. A standard HIPing routine was performed to EBM components and even when pores were visibly reduced, still some remnants persisted.

Solid components showed a characteristic microstructure consisting of acicular α-phase with continuous β interphase showing a more compacted microstructure for samples fabricated with a focus of 30 compared to components fabricated with a focus of 26. It was also observed that cylinders built in a vertical axis, from bottom to top, showed an increase in microstructural size as the cylinder was fabricated. It was also observed that as the melt scan passes were increased the microstructural size increased as well. Mesh components showed a microstructure corresponding to α'-martensitic while foam components showed a mixture of α and α'.

Hardness testing showed no major difference in solid components as the number of melt scan passes was increased, giving a range of 35 to 38 for Rockwell hardness C-scale testing. The same occurred for tensile testing providing a UTS range of 1.1 to 1.4GPa. Mesh components showed an increase in hardness HRC values ranging from 37 to 42 while foam components showed the highest hardness values reaching HRC=42-46. It is stated that as the thickness of the components was reduced, hardness values were increased showing a corresponding microstructural size decrease.

TEM images for solid components of one and three melt scan passes showed the characteristic α-phase surrounded by β-phase, and some dislocation networks formed in one melt scan pass component. On the other side, mesh and foam components showed a corresponding α' microstructure and a mixture of α and α', respectively. It is shown how microstructural features relate to hardness as the cooling rate is changed. In other words, as the cooling rate was increased, by the creation of thinner walls compared to solid components, the microstructural features were enhanced showing finer structures and therefore, a higher hardness was obtained.

From the quality analysis testing results show that coupons or quality tabs that can be easily detached can be used as microstructural reference. This means that actual components can be microstructurally analyzed with what it could be named "non-destructive testing". Results show that detachable tabs have the same microstructure of the component depending on the height of the same. Therefore, components can be analyzed without being destroyed, which can provide helpful microstructural reference for expensive components.

After this research it is fair to say that additive technologies by electron beam melting rapid manufacturing can be suitable for more than one field. It was showed how EBM fabricated components have outstanding properties that can easily be used in different areas. EBM components can improve the biomedical field by the creation of knee and hip implants, as well as other orthopaedic devices such as screws and rods. Besides the biomedical field, complex aerospace components can be created by EBM, that will enhance and reduce the fabrication time since specific dimensions and complex geometries can be created in a single step fabrication process. One last example of a field that can be also benefited is the performing arts such as ballet. EBM manufacturing could revolutionize the already handmade fabrication of pointe shoes utilized. This can enhance the shoe lifetime by the addition of a single box-layer instead of the use of sweat-wettable material.

Even though it has been proven that Ti-6Al-4V manufactured by additive manufacturing by EBM has shown acceptable microstructural and mechanical properties it must be stated that proper testing must be performed to utilize these components in specific situations.

REFERENCES

[1] Long, M. and Rack, H. J. 1998. Titanium Alloys in Total Joint Replacement-A Review. Biomaterials. Vol 19, 1621-1639.

[2] Gibson, I. 2005. Advanced Manufacturing technology for medical applications. London, John Wiley & Sons.

[3] Ashby, M.F., et al. 2000. Metal foams: a design guide. London, Elsevier Science.

[4] Chuna C. K., Leong K. F. and Lim, C. S. 2003.Rapid prototyping: principles and applications. 2nd edition, Singapore, World Scientific.

[5] Froes, F. H. et al., 2004. The technologies of titanium powder metallurgy. Vol 56, No.11, 46- 48.

[6] Hiemenz, J. 2007. Electron Beam Melting. Advanced Materials & Processes. 165. 45-46.

[7] Donachie, M. J. 1982. Titanium and Titanium alloys. American Society for Metals.

[8] Lütjering G. and Williams J. C. 2003. Titanium. Springer.

[9] Oshida Y. 2007. Bioscience and Bioengineering of Titanium Materials. Elsevier.

[10] Li, X., et al. 2009. Fabrication and Characterization of Porous Ti6Al4V Parts for Biomedical Applications Using Electron Beam Melting Process. Materials Letters 63. 403-405.

[11] Cigada, A., Cabrini, M., Pedeferri, P. 1992. Increasing of the Corrosion Resistance of the Ti6Al4V Alloy by High Thickness Anodic Oxidation. Journal of Materials Science: Materials in Medicine 3. 408-412.

[12] Yaszemski, M. J. et al. 2004. Biomaterials in Orthopedics. Marcel Dekker, Inc.

[13] Shanbhag, A., Rubash, H. E. and Jacobs J. J. 2006. Joint Replacement and Bone Resorption, Pathology, Biomaterials, and Clinical Practice. Taylor & Francis.

[14] Kalinyuk, A. N. et al., 2003. Microstructure, Texture, and Mechanical Properties of Electron-beam Melted Ti-6Al-4V. Materials Science and Engineering A346. 178-188.

[15] Christensen, A., Lippincott A. and Kircher R. 2007. Qualification of Electron Beam Melted (EBM) Ti6Al4V-ELI for Orthopaedic Implant Applications. Medical Modeling. 1-7.

[16] Spingborn, R. K. 1967. Non-traditional machining processes. American Society of Tool and Manufacturing Engineers.

[17] Zhuk, H. V., Kobryn, P. A., Semiatin, S. L. 2007. Influence of Heating and Solidification Conditions on the Structure and Surface Quality of Electron-Beam Melted Ti-6Al-4V ingots. Journal of Material Processing Technology 190. 387-392

[18] Ramsdale, R. Engineers handbook. 2004-2006. http://www.engineershandbook.com/RapidPrototyping/ebm.htm

[19] Murr, L.E. et al. 2009. Advanced Metal Powder Based Manufacturing of Complex Components by Electron Beam Melting. Materials Technology. Vol 24, No. 3. 180-190.

[20] Murr, L. E. et al. 2009. Metallographic Characterization of Additive-Layer Manufactured Products by Electron Beam Melting of Ti-6Al-4V Powder. Practical Metallography.

[21] German, R. M. 2005. A Z of Powder Metallurgy. Metal Powders Technology Series: Bernard Williams.

[22] Cansizoglu, O. 2008. Properties of Ti-6Al-4V Non-stochastic Lattice Structures Fabricated Via Electron Beam Melting. Materials Science and Engineering A492. 468-474.

[23] Kobryn, P. A., Semiatin, S.L. 2001. The Laser Additive Manufacture of Ti-6Al-4V. JOM Laser Processing. 40-42.

[24] Becker, W. T. and Shipley, R. J. 2002. Failure Analysis and Prevention. ASM Handbook. Vol 11.

[25] Murr, L. E., et al. 2009. Next Generation Biomedical Implants Using Additive Layered Manufacturing of Complex, Cellular and Functional Mesh Arrays. Philosophical Transactions A. Royal Society, London

[26] Sugui T. et al. 2000. Formation and Role of Dislocation Networks During High Temperature Creep of a Single Crystal Nickel-base superalloy. Materials Science and Engineering. A279. 160-165

[27] Reed-Hill, R. E. and Abbaschian, R. 1994.Physical Metallurgy Principles. International Publishing. 3rd edition.

[28] Amigo, V., et al. 2003. Microstructural Evolution of Ti-6Al-4V during the sintering of microspheres of Ti for orthopedic implants. Journal of Materials Processing Technology 141. 117-122.

[29] Harrysson, Ola, L. A. et al., 2008. Direct Metal Fabrication of Titanium Implants With Tailored Materials and Mechanical Properties Using Electron Beam Melting Technology. Materials Science and Engineering C28. 366-373.

[30] Heinl, P., et al. 2008. Cellular Ti-6Al-4V Structures with Interconnected Macro Porosity for Bone Implants Fabricated by Selective Electron Beam Melting. Acta Biomaterialia 4. 1536-1544.

[31] Javidrad, F. and Rahmati R. 2009. An Integrated Re-engineering Plan for the Manufacturing of Aerospace Components. Materials and Design 30. 1524-1532.

[32] Sparks, J. A. 1997. Low Cost Technologies for Aerospace Applications. Microprocessors and Microsystems 20. 449-454.

[33] Turner, M. W., Schmidt, M. J. J. and Li. L. 2005. Preliminary Study into the Effects of YAG laser Processing of Titanium 6Al-4V Alloy for Potential Aerospace Component Cleaning Application. Applied Surface Science 247. 623-630.

[34] Terlizzi, Jr. et al. 1984. Process of Making a Ballet Toe Shoe. United States Patent 4,453,996.

[35] Cunningham, B. W., et al. 1998. A Comparative Mechanical Analysis of the Pointe Shoe Toe Box. The American Journal of Sports Medicine 26 No. 4. 555-561.

[36] Niinomi, M. 1998. Mechanical Properties of Biomedical Titanium Alloys. Material Science Engineering A243. 231-236.

VITA

Sara Gaytan was born on September 13, 1985 in Chihuahua, Chihuahua, Mexico. Her high school studies were completed at the Preparatoria El Chamizal in Cd. Juarez, Mexico in 2003. Being enrolled in the University of Texas at El Paso for college studies she completed her studies by graduating in May 2008 with a Bachelor's Degree in Metallurgical and Materials Engineering with a specialization in manufacturing. While being an undergraduate she started working as a research assistant in the Metallurgy Department at UTEP.

Permanent address: Paseo 4 #508;
Fracc. Paseo del Rio C.P. 32320
Cd. Juarez, Chihuahua, Mexico

This thesis/dissertation was typed by Sara M. Gaytan.